Optimum Performance-Based Design Of Unsymmetrical 2D Steel Moment Frame

Arezoo Asaad Samani
University of Qom
Seyed Rohollah Hoseini Vaez (hoseinivaez@qom.ac.ir)
University of Qom https://orcid.org/0000-0002-5574-8345
Mohammad Ali Fathali
University of Qom

Research Article

Keywords: Optimization, meta-heuristic algorithms, performance-based seismic design, unsymmetrical 2D steel moment frame

Posted Date: April 30th, 2021

DOI: https://doi.org/10.21203/rs.3.rs-254785/v1

Optimum performance-based design of unsymmetrical 2D steel moment frame

Arezoo Asaad Samani[1]; Seyed Rohollah Hoseini Vaez*[1] and Mohammad Ali Fathali[1]

1 Department of Civil Engineering, Faculty of Engineering, University of Qom, Qom, Iran

*Corresponding author: Seyed Rohollah Hoseini Vaez, S.R. Hoseini Vaez, Department of Civil Engineering, Faculty of Engineering, University of Qom, Qom, Iran E-mail: hoseinivaez@qom.ac.ir

Abstract: The most commonly used analysis method in performance-based design (PBD) is the nonlinear static analysis (NSA). In unsymmetrical 2D frames, unlike its symmetrical state, NSA should be performed in two lateral loading directions, which complicates the process of achieving a feasible optimal design in addition to increasing the volume of calculations. In this study, a two-step approach is proposed for the design of unsymmetrical 2D steel moment-resisting frames (SMRF). In this approach, in two independent steps, the structure is analyzed with lateral loading pattern based on the first mode shape in positive and negative direction, respectively. The implementation of the second step is conditional on the satisfactory completion of the first step. The objective function takes into account the differences between successful and unsuccessful steps. The constraints considered are based on the acceptance criteria for SMRFs according to FEMA-356 at each performance level. The effectiveness of the proposed approach has been investigated by employing four meta-heuristic optimization algorithms to determine the optimum design for case studies of SMRF structures having three and nine stories.

Keywords: Optimization, meta-heuristic algorithms, performance-based seismic design, unsymmetrical 2D steel moment frame**.**

1 Introduction

With the introduction of performance-based design (PBD) to structural and seismic engineering, researchers have focused on improving the reliability of and advancements in this method. The aim of PBD is to enable engineers to design structures that offer predictable performance. The goal is to involve the employer in the selection of the level of building vulnerability at various hazard levels. In conventional structural design methods, a significant aspect of structural performance within the nonlinear limits that entail damage has not been considered. In addition, expectations of structures vary in terms of their importance and uses. However, it is impossible to design a structure that incurs no damage in a disaster and, in many cases, this is not necessary or justifiable. Using PBD, structures can be reviewed to determine their responses under expected earthquakes and engineering judgement modifications can be implemented to improve these responses. PBD has been developed and implemented within the framework of advanced and reliable structural design methods (Gholizadeh and Poorhoseini 2016a). Grierson et al. (2006) employed PBD on steel moment-resisting frames (SMRFs) using modal nonlinear static analysis (NSA) on the dominant modes to assess to the effect of higher modes on a nine-story planar steel frame. Kaveh et al. (2012) used non-dominated sorting genetic algorithm (NSGA-II) for multi-objective

optimization of large performance-based steel structures and were able to reduce the time required for NSA using a simple numerical method. Reduction of the initial and lifecycle costs of large-scale structures were the objective functions for their research. Kaveh and Nasrollahi (2014) assessed PBD of SMRFs for all performance levels by considering inter-story drift as a design criterion. In their study, NSA was carried out using semi-rigid connections and base shear was the criteria used to determine performance levels. Gholizadeh (2015) used the target displacement for determining performance levels that was calculated by the equation recommended in FEMA-356. In this study, the structure initially was controlled against the gravity load. If the member resistance was sufficient, NSA was conducted. Gholizadeh and Milani (2016) used nonlinear time-history analysis to determine structural responses. They used a combination of a radial basis function neural network (RBF) and optimization algorithms for their design. Gholizadeh and Baghchevan (2017) employed PBD for a SMRF using a multi-objective optimization algorithm. Initially, geometric and strength constraints were controlled under gravity loads and, if geometric and strength controls were satisfactory, NSA was carried out to assess maximum inter-story drift as another constraint. Karimi and Hoseini Vaez (Karimi and Vaez 2019) proposed a two-stage optimal seismic design of SMRFs in which the requirements of the LRFD method initially were controlled and then the PBD method was applied based on the target roof displacement. Additional studies have been conducted on the use of PBD for steel frames (Fathali and Hoseini Vaez 2020; Gholizadeh and Ebadijalal 2018; Gholizadeh and Poorhoseini 2016b; Mergos 2018; Shoeibi et al. 2018). Optimization of this type of design adds to the important economic aspect of PBD. Engineering optimization issues can be too complex to solve using conventional optimization methods; thus, meta-heuristic algorithms have been developed to solve them. These algorithms are capable of solving several optimization problems (Aljarah et al. 2018; Arora and Singh 2019; Fathollahi-Fard et al. 2020; Ghasemi-Marzbali 2020; Heidari et al. 2019; Kaveh et al. 2017; Mirjalili et al. 2014; Mohammad Rezapour Tabari and Hashempour 2019). In some PBD studies, base shear has been used to determine the performance levels. The current study has used target displacement to determine performance levels. Because the most common analytical method for assessing seismic performance is NSA, this method has been used as the basis of structural analysis. Previous studies have assessed symmetrical 2D frames and displacement of the control node in NSA in one direction. However, in 2D unsymmetrical frames, it is necessary to conduct NSA in both directions. The consideration of both directions increases the optimization process; thus, less attention has been paid to optimization of unsymmetrical SMRFs using PBD. In this study, a two-step approach is proposed for decreasing the optimization process of the optimal design of unsymmetrical 2D SMRFs based on PBD. The aim of optimization is to reduce the structural weight and uniform inter-story drift distribution while satisfying the acceptance criteria for each performance level. In some studies, constraints such as controlled inter-story drift, strength, and limits on rotational plastic hinges have not been considered; however, the present study has defined the constraints based on SMRF acceptance criteria as defined in FEMA-356 (2000). The Salp Swarm Algorithm (SSA), Enhanced Colliding Bodies Optimization algorithm (ECBO), Enhanced Vibrating Particles System algorithm (EVPS) and Enhanced Whale Optimization Algorithm (EWOA) were used to optimize two 2D SMRFs in order to assess the optimal PBD.

2 Optimum performance-based design

2.1 PBD concept

PBD includes the design of the structural members based on the expected performance of the structure under specific types of earthquakes.

In order to determine the design objectives, the structural performance level and the seismic hazard level should be determined. The current study used the immediate occupancy (IO), life safety (LS), and collapse prevention (CP) performance levels from FEMA-356 based on the enhanced rehabilitation concept at 20%, 10%, and 2% earthquake probability over 50 years, respectively. Because NSA was used, the structure was subjected to a specific lateral load distribution (first mode of structural vibration) until the lateral displacement of the control point reached the target displacement. The amount of target displacement at each performance level based on FEMA-356 can be calculated as:

$$\delta_t = C_0 C_1 C_2 C_3 S_a \frac{T_e^{\,2}}{4\pi^2} g \tag{1}$$

where C_0 is the spectral displacement of an equivalent single-degree of freedom system related to the roof displacement multi-degree of freedom system of the building, C_1 is the expected maximum inelastic displacement related to the displacement for the linear elastic response, C_2 is the effect of strength and stiffness degradation and pinched hysteretic shape on the maximum displacement response, and C_3 is the increased displacement due to dynamic P-Δ effects. In Eq. (1), S_a is the response spectrum acceleration corresponding to effective fundamental period T_e and g is the acceleration of gravity. Spectral acceleration is the specific elastic design spectrum of the site at a specific period for a specific damping ratio. Spectral acceleration (S_a) for all three performance levels at 5% effective damping can be calculated as:

$$S_a^i = \begin{cases} F_a S_s^i \left(0.4 + 3T_e / T_0\right) & 0 < T_e \le 0.2T_0^i \\ F_a S_s^i & 0.2T_0^i < T_e \le T_0^i \\ F_v S_1^i / T_e & T_e > T_0^i \end{cases} \tag{2}$$

$$T_0^i = (F_v S_1^i)/(F_a S_s^i), \quad i = IO, LS, CP$$

where S_1 and S_S are the response acceleration parameters for a 1-sec period and for a short-period (0.1 sec), respectively, and F_a and F_v are the site class coefficients based on FEMA-356. In PBD, each element action is classified as either deformation-controlled or force-controlled and the acceptance criteria are defined in accordance with this. The acceptance criteria should be controlled in the target displacement of each performance level for all members.

2.2 Optimization problem formulation

Each optimization problem has three parts: optimization variables (design variables), objective function, and constraints. In this study, the design variables were selected for W-shaped steel sections according to the AISC design manual (LRFD-AISC 2001).

2.2.1 Objective function formulation

In addition to minimizing the building weight, uniform inter-story drift distribution was also assessed. Therefore, according to Eq. (3), the objective function consists of two terms (Grierson et al. 2006):

$$F(\boldsymbol{X}) = F_1(\boldsymbol{X}) + F_2(\boldsymbol{X}) \tag{3}$$

where F_1 is the normalized building weight and is formulated as:

$$F_1(\boldsymbol{X}) = \frac{1}{W_{\max}} \sum_{i=1}^{ng} \rho_i A_i \sum_{j=1}^{nm} L_j \tag{4}$$

where $W_{\max}$ is the weight of the building which includes the heaviest sections of final section list of element groups, nm is the number of structural elements that are collected in ng design groups, ρ_i and A_i are the weight of the unit volume and cross-sectional area of the i^{th} group section, respectively, and L_j is the length of the j^{th} element in the i^{th} group. In Eq. (3), F_2 is the second term of the objective function for considering the uniform inter-story drift distribution and is defined as:

$$F_2(\boldsymbol{X}) = \left[\frac{1}{n_s} \sum_{s=1}^{n_s-1} \left(\frac{\upsilon_s^{CP}(\boldsymbol{X})/H_S}{\Delta^{CP}(\boldsymbol{X})/H} - 1 \right)^2 \right]^{1/2} \tag{5}$$

where n_s is the number of building stories, υ_s^{CP} and Δ^{CP} are the drift of story s and the roof drift at the CP performance level, respectively, H is the height of the building, and H_s is the vertical distance from the base of the building to story s. The optimization problem then can be formulated as:

$$\begin{aligned} &\text{Find: } \boldsymbol{X} = \left\{ x_1, x_2, x_3, ..., x_{ng} \right\}^T \\ &\text{To minimize: } F(\boldsymbol{X}) = F_1(\boldsymbol{X}) + F_2(\boldsymbol{X}) \\ &\text{Subject to: } g_j(\boldsymbol{X}) \le 0, \quad j = 0,1,2,...,nc \end{aligned} \tag{6}$$

where $\boldsymbol{X}$ is the vector of the design variables, $F(\boldsymbol{X})$ is the objective function, $g_j(\boldsymbol{X})$ is the j^{th} design constraint, and nc is the number of constraints. The constraints of the optimization problem are applied on the objective function based on the exterior penalty function method and is expressed as:

$$\begin{aligned} &\varphi(\boldsymbol{X}, r) = F(\boldsymbol{X}) \left(1 + r \sum_{j=1}^{nc} V_j^2 \right) \\ &V_j = \max\left\{ 0, g_j(\boldsymbol{X}) \right\} \end{aligned} \tag{7}$$

where φ and r are the pseudo-objective function and the positive penalty parameter, respectively, and V_j is the violation of the j^{th} constraint.

2.2.2 Constraints

According to FEMA-356 for SMRFs, the flexural behavior of the beams should be deformation-controlled. In steel columns, whenever the axial force is less than 50% of the lower-bound axial compression strength of the column (P_{CL}), the flexural and axial behavior of the column should be considered to be deformation-controlled and force-controlled, respectively.

The constraint corresponding to the plastic rotation of plastic hinges is defined as:

$$\begin{aligned} &g_{i,d}^{\theta} = \left(\left| \theta_{P,d}{}^i \right| / \theta_{all,d}{}^i \right) - 1 \le 0 \\ &i = IO, LS, CP, \quad d = 1,2,...,nh \end{aligned} \tag{8}$$

where $\theta_{P,d}{}^i$ and $\theta_{all,d}{}^i$ are the plastic rotation of the d^{th} plastic hinge and its allowable values at the i^{th} performance level based on FEMA-356, respectively, and nh is the number of plastic hinges. In steel columns with axial compressive forces that are more than 50% of the P_{CL}, both the axial loads and flexure shall be considered to be force-controlled. According to FEMA-356, the constraint for such columns at the CP performance level is:

$$\begin{aligned} &g_j^s = \left[\left(P_{UF,j} / P_{CL,j} \right) + \left(M_{U,j} / M_{CL,j} \right) \right] - 1 \le 0 \\ &for \ P_{UF,j} / P_{CL,j} > 0.5, \quad j = 1,2,...,nf \end{aligned} \tag{9}$$

where g_j^s is the strength constraint of the j^{th} column, nf is the number of columns, $P_{UF,j}$ and $M_{U,j}$ are the axial force and bending moment of the j^{th} column derived from analysis, respectively, and $M_{CL,j}$ is the lower-bound flexural strength of the j^{th} column. In order to satisfy the criteria for the design of the column-column and beam-column joints in steel structures, the geometric constraints should be controlled as (Gholizadeh and Baghchevan 2017):

$$g_{G,k} = \begin{cases} \left(b_B / b_C^{bot} \right)_k - 1 \le 0 \\ \left(h_C^{top} / h_C^{bot} \right)_k - 1 \le 0 \end{cases}, \quad k = 1,...,nk \tag{10}$$

where $g_{G,k}$ is the geometric constraint of the k^{th} connection, b_B and $b_C{}^{bot}$ are the flange width of the beam and flange width of the bottom column for the k^{th} connection, respectively, $h_C{}^{bot}$ and $h_C{}^{top}$ are the depth of the bottom and top columns for the k^{th} connection, respectively, and nk is the number of joints. The constraint for the slenderness ratio of the column (λ) is:

$$g_j^{\lambda} = \frac{\left(K_j l_j / r_j \right)}{200} - 1 \le 0, \quad j = 1,2,...,nf \tag{11}$$

where K_j, l_j and r_j are the effective length factor, unsupported length, and cross-section gyration

radius of the j^{th} column, respectively. The inter-story drift constraint at each performance level is:

$$g_{j,i}^{\Delta} = \left(\Delta_j^i / \Delta_{all}^i\right) - 1 \le 0$$
$$i = IO, LS, CP \quad , \quad j = 1,2,...,n_s \tag{12}$$

where $\Delta_j{}^i$ and $\Delta_{all}{}^i$ are the inter-story drift of the j^{th} story and the allowable inter-story drift at i^{th} performance level, respectively. The allowable inter-story drift (Δ_{all}) was considered to be 0.012, 0.031, and 0.061 of the story height for the IO, LS and CP performance levels, respectively (Gong 2004; Karimi and Vaez 2019).

2.2.3 Reducing the search space

In order to improve the optimization process before the beginning of the optimization, an approach was used to reduce the search space as much as possible and increase the ability of the algorithm to achieve a solution. In this approach, a number of column sections with minimum effective length coefficients greater than the allowable value are removed from the sections list of the columns group and the search space was decreased. The proposed approach for reducing the search space is defined according to the flowchart shown in Fig. 1. The equations in Fig. 1 are as follows:

$$K = \sqrt{\frac{1.6G_AG_B + 4.0(G_A + G_B) + 7.5}{G_A + G_B + 7.5}} \tag{13}$$

where K is the column effective length factor. In Eq. (13), the value of G for the joints at both ends of each column (G_A and G_B) can be calculated using Eq. (14). If the column end is rigidly attached to a properly designed footing, this value is considered to be unity.

$$G = \sum\left(\frac{E_cI_c}{L_c}\right) \Big/ \sum\left(\frac{E_bI_b}{L_b}\right) \tag{14}$$

In this equation, I_c, E_c, and L_c are the moment of inertia, modulus of elasticity, and unsupported length of the column, respectively, and I_b, E_b, and L_b are the same parameters for the beam under consideration.

2.2.4 Proposed Approach

The structure was analyzed using NSA under gravity and lateral loads, which is considered to be the first mode for the lateral loading pattern. Fig. 2 shows how to apply lateral loading pattern based on the first mode shape in positive and negative direction to the structures. When the constraints were satisfied in the positive direction under NSA, the structure next underwent NSA with the lateral loading pattern in the negative direction and the constraints were controlled in this direction. When the constraints were satisfied in the second direction, the solution was deemed to be acceptable; however, if the constraints were not satisfied in the first direction, the second direction was not assessed. OpenSees software (2016) was used for the NSA which is an open-source software framework for finite element analysis (Mazzoni et al. 2005). Fig. 3 shows the flowchart for each stage in which parameter *NS* is an additional penalty coefficient, the value of which depends on the satisfactory fulfillment of each step. Three target roof displacements (0.007, 0.025, and 0.05 of the total height of the structure) which corresponded to the performance levels for IO, LS, and CP, respectively, were selected as the initial assumptions for bilinearization.

3 Meta-heuristic algorithms

The use of meta-heuristic algorithms to solve optimization problems is a common approach in research. The ability of these algorithms to cover a search space and escape from local optima lead to suitable results.

3.1 Salp Swarm Algorithm

Mirjalili et al. (2017) presented a Salp Swarm Algorithm (SSA) based on the swarming behavior of salps (Anderson and Bone 1980; Madin 1990). In order to form a mathematical model for a salp chain, the population initially should be divided into two

groups: a leader and the followers. An n-dimensional search space is considered for salp position $\boldsymbol{x}$ in which n represents the number of problem variables and food source F is the swarm target.

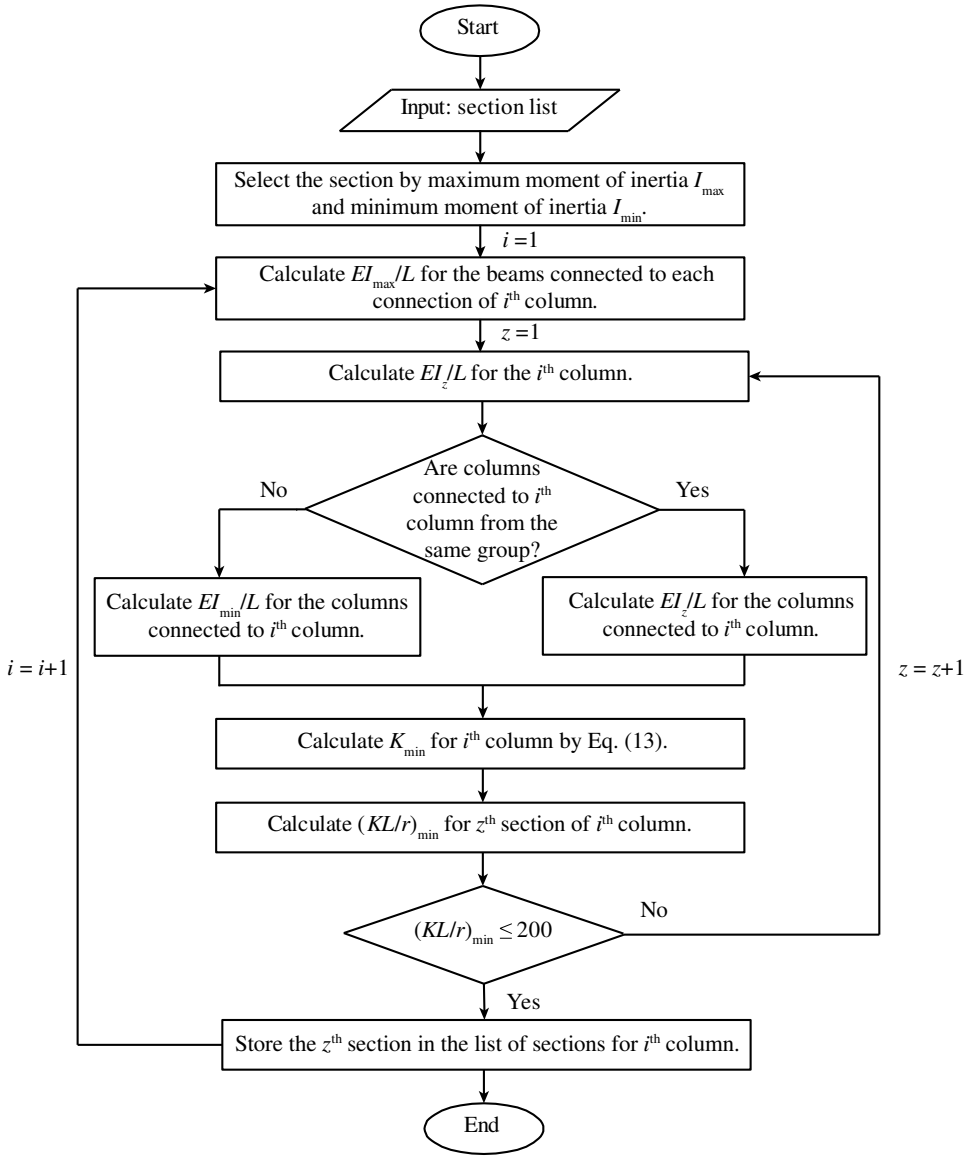

Fig. 1 Flowchart for reducing the search space

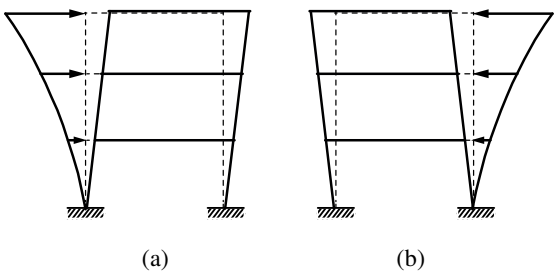

Fig. 2 Lateral loading pattern based on the first mode shape (a) in positive direction and (b) in negative direction

The SSA algorithm stores the best solution and allocates it to the food source position. The leader always explores and exploits the space around the food source. SSA updates the position of followers based on their positions and that of the leader. The gradual movement of the followers prevents them from exiting the search space. Fig. 4 shows the flowchart of the SSA. The equations mentioned in the flowchart are as follows:

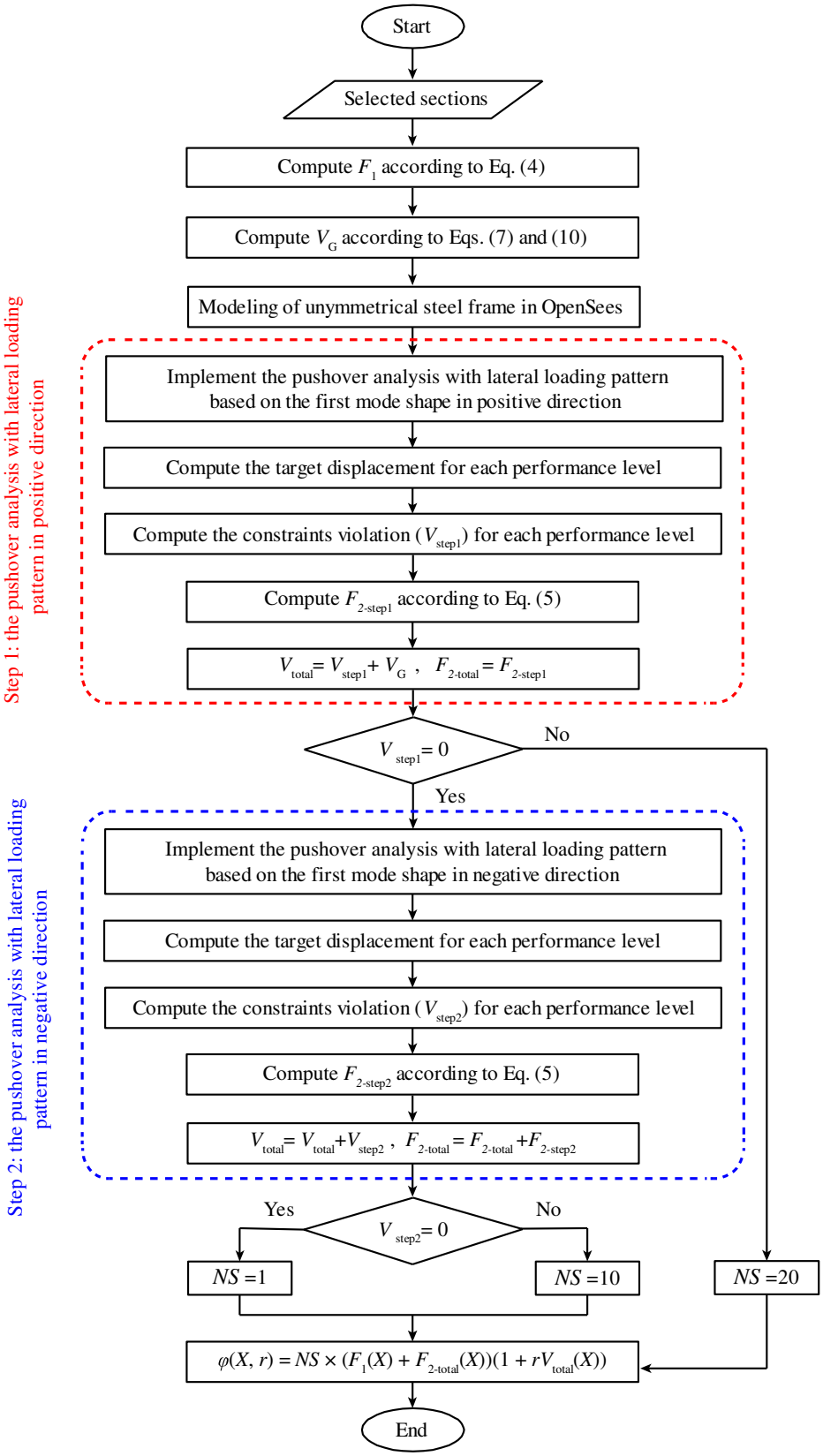

Fig. 3 Flowchart of proposed approach

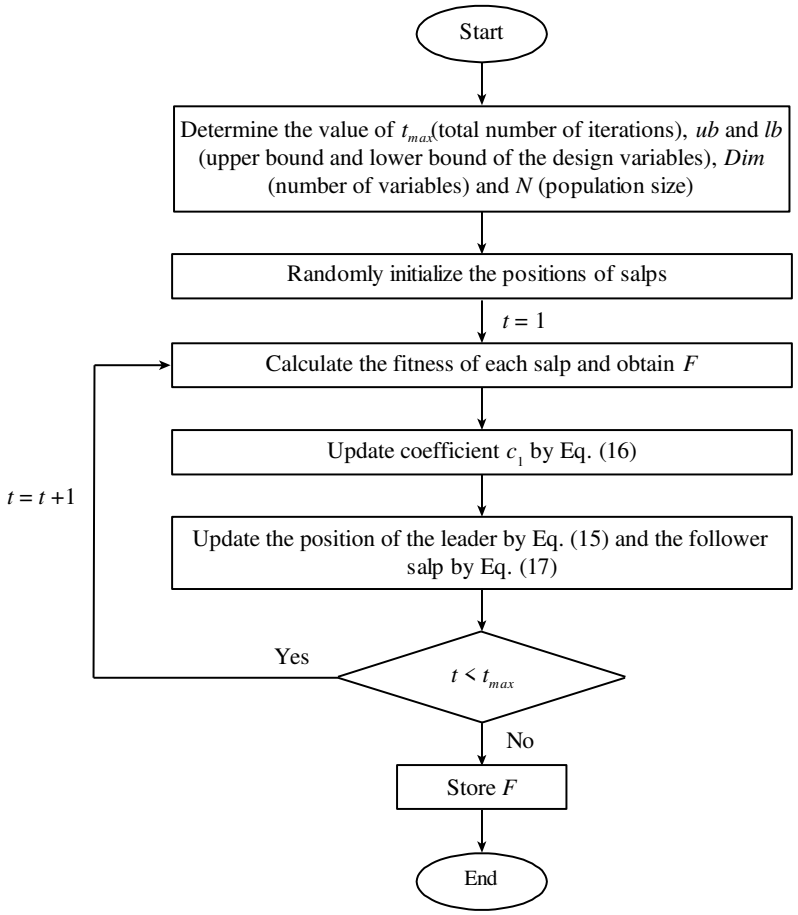

Fig. 4 Flowchart of SSA algorithm

$$\boldsymbol{x}_j^1 = \begin{cases} F_j + c_1\left(\left(ub_j - lb_j\right)c_2 + lb_j\right) & c_3 \geq 0.5 \\ F_j - c_1\left(\left(ub_j - lb_j\right)c_2 + lb_j\right) & c_3 < 0.5 \end{cases} \quad (15)$$

In Eq. (15), $\boldsymbol{x}_j^1$ is the position of the leader, F_j is the position of the food source in the j^{th} dimension, ub_j and lb_j are the upper and lower bounds in the j^{th} dimension, respectively, and c_2 and c_3 are random numbers that are generated uniformly in the [0,1] interval; and c_1 is:

$$c_1 = 2e^{-(4t/t_{\max})^2} \quad (16)$$

where t is the number of current iterations, and t_{max} is the maximum iteration; and:

$$\boldsymbol{x}_j^i = 0.5\left(\boldsymbol{x}_j^i + \boldsymbol{x}_j^{i-1}\right) \quad (17)$$

where, for $i \geq 2$, $\boldsymbol{x}_j^i$ is the position of the i^{th} follower in the j^{th} dimension. The salp chain can be modelled using Eqs. (15) and (17).

3.2 Enhanced Colliding Bodies Optimization algorithm

Kaveh and Ilchi Ghazaan (2014) proposed the Enhanced Colliding Bodies Optimization (ECBO) algorithm to improve the convergence rate of CBO by adding a memory to store some of the best solutions during optimization along with the objective function values and their related mass. The solution vectors stored in the memory are added to the population and an equivalent number of existing worst states CBs are deleted. The CBs are sorted in descending order based on their mass. Fig. 5 shows the pseudo-code of the ECBO. The equations in the pseudo-code are listed in Table 1.

Determine the value of maximum number of iterations (t_{max}), population size (N) and colliding memory size.
Define the *Pro* in the [0, 1] range.
Initialize the position of CBs randomly in the search space.
While $t < t_{max}$
  Calculate the coefficient of restitution (ε) by Eq. (T1)*.
  Evaluate the objective function of CBs (f).
  Calculate the value of mass matrix (**m**) for the CBs using Eq. (T2).
  Update colliding memory and population.
  Divide CBs into stationary and moving groups and calculate their velocities before collision (**v**) by Eqs. (T3) and (T4).
  Calculate CBs velocities after the collision (**v'**) by Eqs. (T5) and (T6).
  Update the position of each CB by Eqs. (T7) and (T8).
  Select a random number (*rni*) that is distributed in the [0, 1] range.
  for **i=1:N**
    if *rni*<*Pro*
      Select one dimension of the i^{th} CB randomly and recalculate its value by Eq. (T9).
    end
  end
end
Report the best solution found by the algorithm.

* Eqs. (T1) to (T9) defined in Table 1

Fig. 5 Pseudo-code for ECBO algorithm

Table 1 Equations in ECBO pseudo-code

Equation tag	Equations
(T1)	$\varepsilon = 1 - \left(t / t_{\max}\right)$
(T2)	$m_k = \left(1/f\ (k)\right) \Big/ \sum_{i=1}^{N} \left(1/f\ (\boldsymbol{X}_i)\right)$
(T3)	$\boldsymbol{v}_i = 0$, $i = 1, 2, \ldots, N/2$
(T4)	$\boldsymbol{v}_i = \boldsymbol{x}_i - \boldsymbol{x}_{i-(N/2)}$, $i = N/2+1, N/2+2, \ldots, N$
(T5)	$\boldsymbol{v'}_i = \left[(1+\varepsilon) m_{i+(N/2)} \Big/ \left(m_i + m_{i+(N/2)} \right) \right] \boldsymbol{v}_{i+(N/2)}$, $i = 1, 2, \ldots, N/2$
(T6)	$\boldsymbol{v'}_i = \left[\left(m_i - \varepsilon m_{i-(N/2)} \right) \Big/ \left(m_i + m_{i-(N/2)} \right) \right] \boldsymbol{v}_i$, $i = N/2+1, N/2+2, \ldots, N$
(T7)	$\boldsymbol{x}_i^{new} = \boldsymbol{x}_i + \boldsymbol{rand} \circ \boldsymbol{v'}_i$, $i = 1, 2, \ldots, N/2$
(T8)	$\boldsymbol{x}_i^{new} = \boldsymbol{x}_{i-(N/2)} + \boldsymbol{rand} \circ \boldsymbol{v'}_i$, $i = N/2+1, N/2+2, \ldots, N$
(T9)	$\boldsymbol{x}_i{}^j = \boldsymbol{x}_{\min}{}^j + rand \,.\left(\boldsymbol{x}_{\max}{}^j - \boldsymbol{x}_{\min}{}^j \right)$

- t is the current iteration number.
- ***rand*** is a random vector with a dimension of the number of problem variables, consisting of random numbers in the interval of
- [-1, 1].
- $\boldsymbol{x}_i{}^j$ is the value of the j^{th} variable of the i^{th} CB.
- $\boldsymbol{x}_{\max}{}^j$ and $\boldsymbol{x}_{\min}{}^j$ are the upper and lower bounds of the j^{th} variable, respectively.
- *rand* is a random vector in the [0, 1] range.

3.3 Enhanced Vibrating Particles System algorithm

The Enhanced Vibrating Particles System (EVPS) algorithm is an alternative to the VPS algorithm that features an increased convergence rate and improved VPS algorithm efficiency (Kaveh et al. 2018). The VPS is a meta-heuristic algorithm based on the free vibration of a single degree of freedom system (Kaveh and Ghazaan 2017).

The parameters of this meta-heuristic algorithm are:

- OHB: One of the best positions generated of the entire population until the current iteration. It is a row of memory that is randomly selected.
- GP: An appropriate particle that is randomly selected from the best solutions in each iteration.
- BP: An inappropriate particle that is randomly selected from the worst solutions in each iteration.

In this algorithm, the memory parameter stores the best positions of the entire population generated prior to the current iteration with the same memory matrix dimensions. The position of particles in the EVPS algorithm can be updated by Eq. (18). In Eq. (18), one of the (a) to (c) equations is selected based on the probability of ω_1 to ω_3, respectively; *BP*, *GP*, and *OHB* are determined independently for each particle; ω_1, ω_2 and ω_3 are the relative importance of *OHB*, *GP* and *BP*, respectively.

$$\boldsymbol{x}_i^j = \begin{cases} \left[D.A.rand1 + OHB^j \right] \\ \left[D.A.rand2 + GP^j \right] \\ \left[D.A.rand3 + BP^j \right] \end{cases}$$

$$A = \begin{cases} (-1)^{round(rand)} \left(OHB^j - \boldsymbol{x}_i^j \right) & (a) \\ (-1)^{round(rand)} \left(GP^j - \boldsymbol{x}_i^j \right) & (b) \\ (-1)^{round(rand)} \left(BP^j - \boldsymbol{x}_i^j \right) & (c) \end{cases} \qquad (18)$$

$$\omega_1 + \omega_2 + \omega_3 = 1$$

where, *rand*, *rand*1, *rand*2, and *rand*3 are random numbers that are uniformly distributed in the [0, 1] interval, and *D* is the damping surface modeling parameter in the vibration which is defined as:

$$D = \left(t / t_{\max} \right)^{-\alpha} \qquad (19)$$

where t is the current number of iterations, $t_{\max}$ is the total number of iterations, and α is a constant value. The *HMCR* parameter determines whether a violating component should change in response to value changes in *OHB* or be selected from the allowable search space. If the *OHB* value changes, another parameter (*PAR*) will be used to determine whether or not the value should change with the neighbouring value.

3.4 Enhanced Whale Optimization Algorithm

The Enhanced Whale Optimization Algorithm (EWOA) (Kaveh and Ilchi Ghazaan 2017) has also been used in the present study. This algorithm was developed to enhance the rate of convergence and reliability of the WOA, which was inspired by the hunting of humpback whales and is known as a bubble-net hunting strategy. The flowchart for EWOA is shown in Fig. 6. The equations of this flowchart are as follows:

$$\begin{aligned} &\boldsymbol{X}(t+1) = \boldsymbol{X}(t) - \mathbf{A} \, o \boldsymbol{D}''' \\ &\boldsymbol{D}''' = \boldsymbol{r} \, o \left| \boldsymbol{X}(t) \right|, \quad \boldsymbol{a} = 2\boldsymbol{a} \, or \, -\boldsymbol{a} \end{aligned} \qquad (20)$$

where $\boldsymbol{r}$ is a random vector containing arrays that are uniformly distributed in interval [0,1], $\boldsymbol{a}$ is a vector of numbers which decrease in linear order in interval [0,2] during the iterations, $\boldsymbol{X}$ is a vector indicating the position of the whale, and t is the number of the current iterations; and:

$$\begin{aligned} &\boldsymbol{X}(t+1) = e^{bk} . \cos(2\pi k) . \boldsymbol{D}' + \boldsymbol{X}^*(t) \\ &\boldsymbol{D}' = \left| \boldsymbol{X}^*(t) - \boldsymbol{X}(t) \right| \end{aligned} \qquad (21)$$

where b is a constant number used to define the logarithmic spiral shape, k is a random number which is uniformly distributed in interval [-1, 1], and $\boldsymbol{X}^*$ is the current best position of the whale; and:

$$p = 0.3\left(1 - t / t_{\max}\right)$$

where t and $t_{\max}$ denote the current iteration and number of total iterations in the optimization process, respectively.

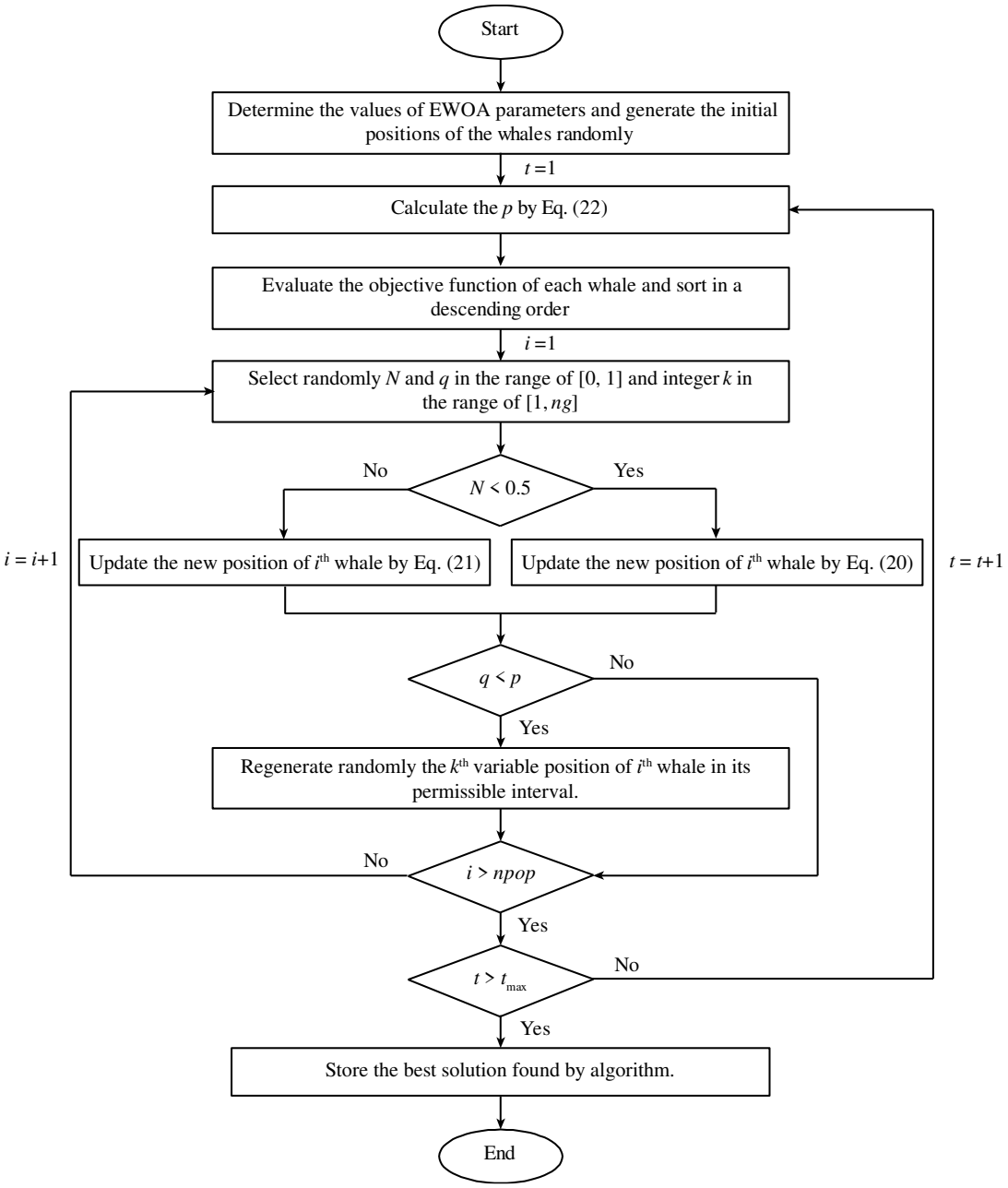

Fig. 6 Flowchart of EWOA algorithm

4 Numerical examples

Two numerical examples were considered to investigate the optimum PBD of unsymmetrical SMRFs using the SSA, ECBO, EVPS and EWOA. As meta-heuristic algorithms are based on stochastic search in finding the optimal answer, different random seeds are generated in each run, which causes scattering in the results. For this reason and in order to assess the scattering of the results, the optimization of each example was performed in 30 independent runs. Hasan et al. (2002) and Hassan et al. (2005) used a symmetrical shape for these frames to conduct NSA. Kaveh et al. (2010) used them for optimal design and Kaveh and Nasrollahi (2014) assessed the performance of the CSS algorithm for the optimal design of these frames. The frames were considered to be unsymmetrical for optimal PBD.

The unsymmetry of the frames was caused the difference in the end bay length compared to the other bays. The length of each bay was 9.15 m and the height of each story, except for the end bay, was 3.96 m. The length of the end bay was 7.62 m. The expected yield strength (F_{ye}) of the steel for the columns and beams was 397 and 339 MPa, respectively. The modulus of elasticity (E) was 200 GPa. The column section list was limited to wide-flange sections W8 to W14 and the beam sections were selected as all W-shaped sections. The values for parameters S_1, S_S, F_a and F_v are listed in Table 2.

Table 2 Site parameters for site class of D (Kaveh et al. 2010)

Performance level	Hazard level	S_s (g)	S_1 (g)	F_a	F_v
IO	20%/50-years	0.658	0.198	1.27	2.00
LS	10%/50-years	0.794	0.237	1.18	1.92
CP	2%/50-years	1.150	0.346	1.04	1.70

4.1 Three-story, four-bay steel frame

Fig. 7 shows the grouping of elements and applied loads for the three-story steel frame. Fig. 8 shows the number of hinges. A constant gravity load of W_1 = 32 kN/m was applied to the first and second stories and a constant gravity load of W_2 = 28.7 kN/m was applied to the beams of the roof. The seismic weight for the first and second stories was 4688 kN and for the third story was 5071 kN.

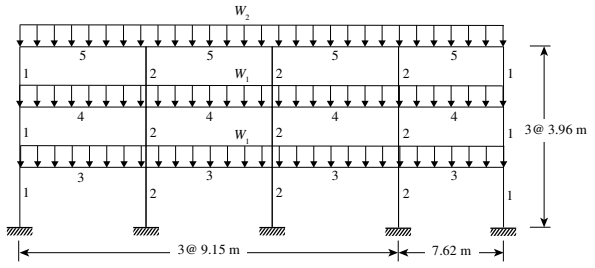

Fig. 7 Geometry, loading and grouping of the elements of 3-story steel frame

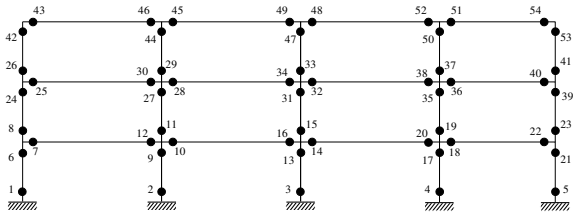

Fig. 8 Number of potential plastic hinges in 3-story steel frame

For each optimization algorithm in this problem, a population of 60 and a maximum of 300 iterations were considered. Table 3 presents the optimum sections and the best, worst, average, standard deviation and coefficient of variation of weights of the structure obtained from each of the optimization algorithms.

Table 3 Optimal sections and weights for 3-story frame

Element group	ECBO	EVPS	EWOA	SSA
1	W12 × 120	W12 × 120	W14 × 233	W14 × 159
2	W14 × 233	W14 × 193	W12 × 136	W14 × 193
3	W27 × 102	W27 × 114	W33 × 130	W30 × 116
4	W30 × 99	W30 × 99	W30 × 118	W27 × 102
5	W14 × 61	W12 × 58	W10 × 77	W10 × 100
Best weight (kN)	297.13	280.94	318.08	318.79
Worst weight (kN)	649.67	457.38	546.49	486.90
Average weight (kN)	427.14	372.05	411.25	397.62
Standard deviation of weights (kN)	96.56	50.32	68.79	71.91
Coefficient of variation (%)	22.61	13.53	16.73	18.08

Fig. 9 compares the ratio of the best solution to those obtained from the different algorithms in 30 independent runs. As the ratio increased, the difference between the best solution and the solutions achieved from the different runs decreased and a better solution was obtained. It can be seen that EVPS was more capable of finding the optimal solution.

The optimum weight of the structure and the objective function value obtained by this algorithm were 280.94 kN and 0.147, respectively. As the scattering decreased in each chart, the performance of the algorithms became more uniform for the optimal solution from each independent run. Fig. 9 and Table 3 indicate that EVPS exhibited less scattering caused by random seed in the results of each independent run. This indicates its more uniform performance in comparison with the other algorithms.

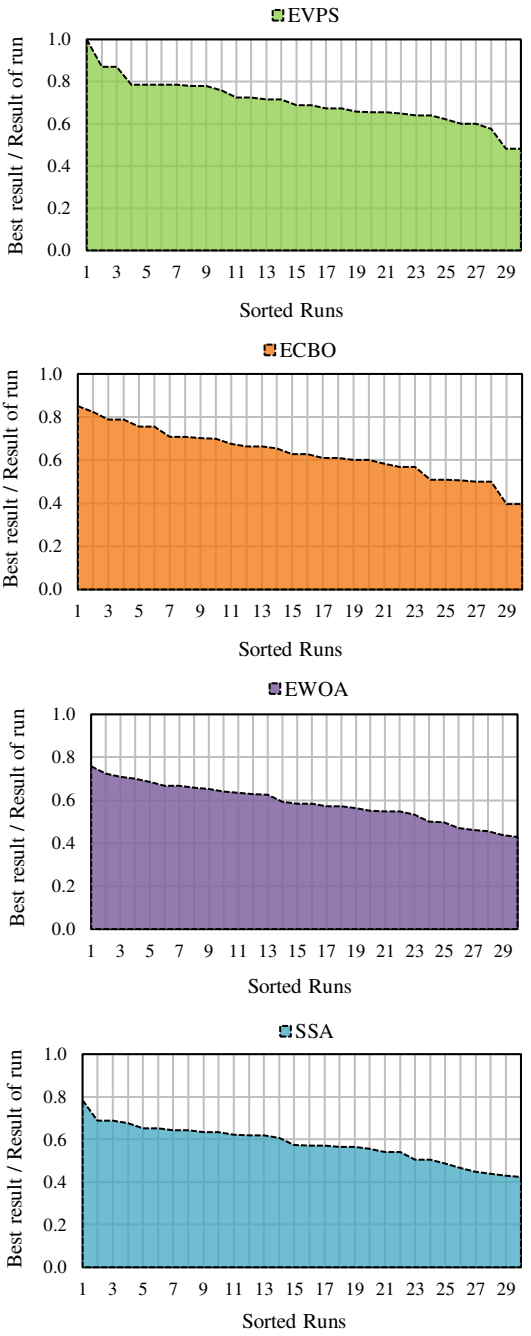

Fig. 9 Ratio of best solution to solution of each algorithm for 3-story steel frame

Fig. 10 and 11 show the formation patterns of plastic hinges in the optimal solution for the 3-story frame using NSA with lateral loading pattern based on the first mode shape in positive and negative direction, respectively at each performance level. Fig. 12 shows the ratio of plastic hinge rotation to their allowable values according to FEMA 356 for nonlinear analysis of the 3-story frame at the mentioned load patterns. As can be observed, this ratio was smaller than unity for all plastic hinges, which indicates an acceptable amount of plastic hinge rotation (plastic hinge rotations which were negligible are not shown). The formation pattern and rotation of the plastic hinges in the unsymmetrical 3-story structure at different performance levels confirm that NSA should be performed in both directions to obtain accurate and reliable results.

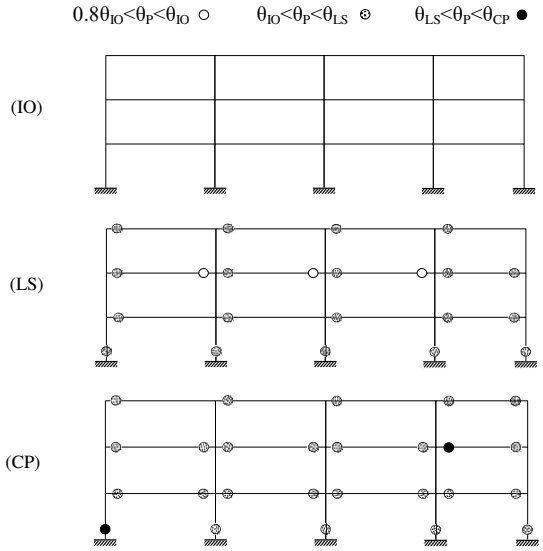

Fig. 10 Plastic hinges formation for a 3-story frame with lateral loading pattern based on the first mode in positive direction

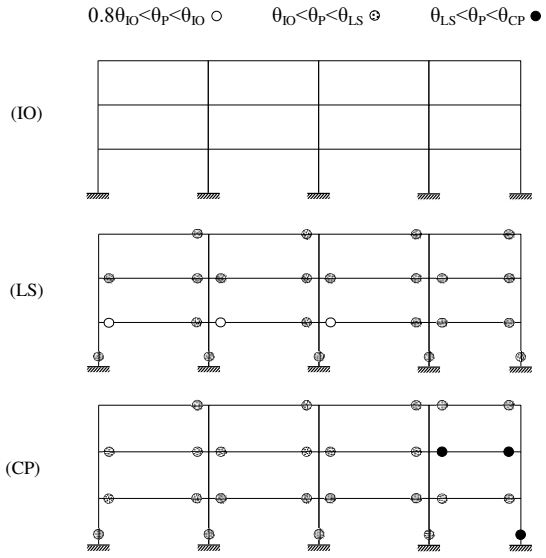

Fig. 11 Plastic hinges formation for a 3-story frame with lateral loading pattern based on the first mode in negative direction

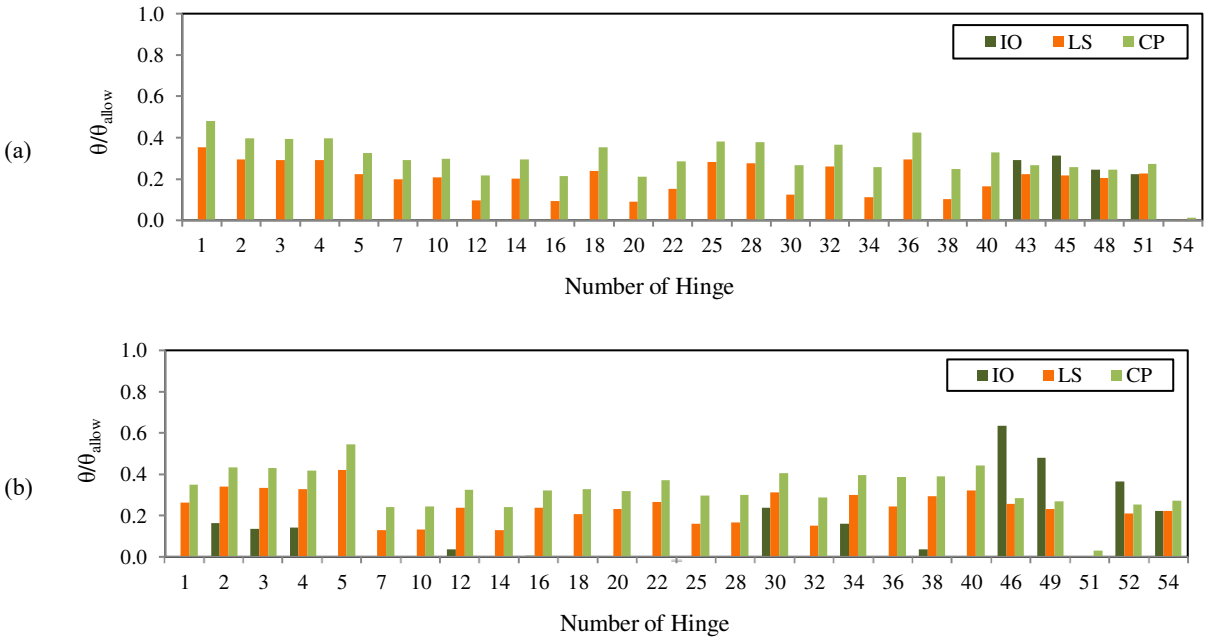

Fig. 12 Ratio of plastic rotation of hinges to their allowable values for 3-story steel frame with lateral loading pattern based on the first mode shape in: (a) positive direction; (b) negative direction

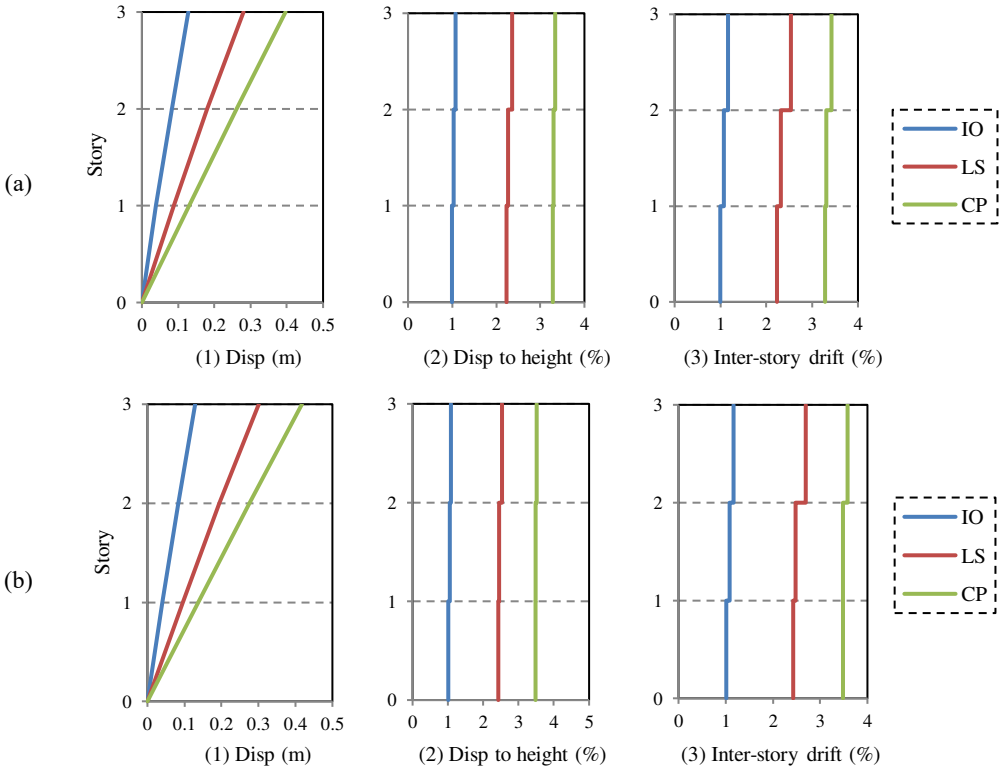

Fig. 13 Results of story drift for 3-story frame with lateral loading pattern based on the first mode shape in: (a) positive direction; (b) negative direction

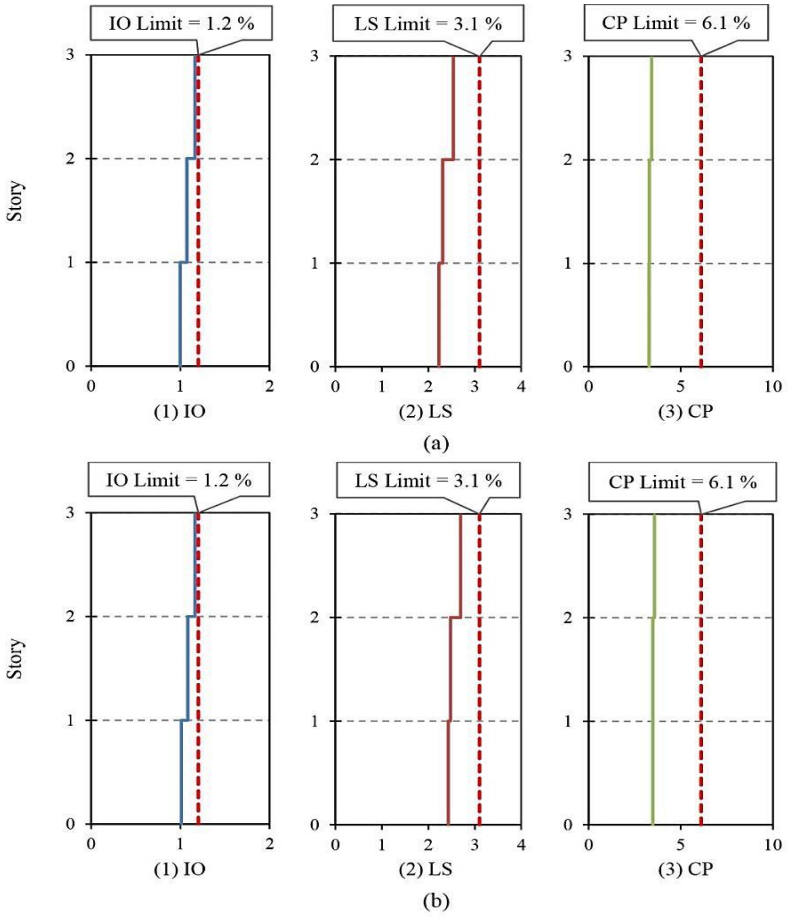

Fig. 14 Comparison of inter-story drift ratios (%) and their permitted values for best solution for a 3-story steel frame with lateral loading pattern based on the first mode shape in: (a) positive direction; (b) negative direction

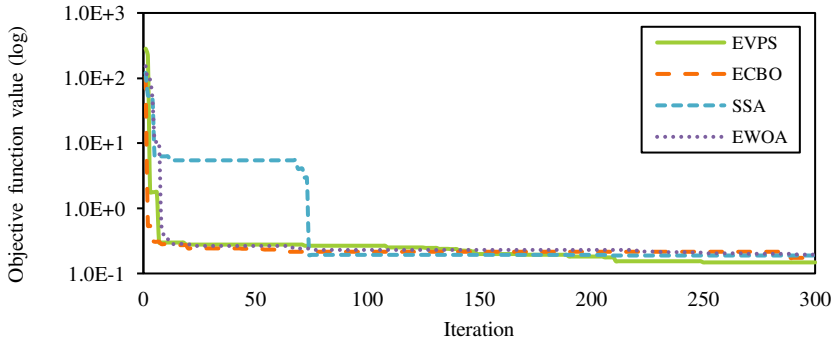

Fig. 15 Convergence curve of best solution of each algorithm for 3-story steel frame

Fig. 13 shows the displacement (Disp) of the stories, the displacement-to-height ratio, and the inter-story drift ratio of the structure for both load patterns. Fig. 14 compares the inter-story drift ratios and their permitted values for the best solution. Fig. 15 shows the optimization convergence of the best answer for each algorithm.

4.2 Nine-story, five-bay steel frame

Fig. 16 shows the geometry, grouping of elements, and applied loads for a nine-story, five-bay steel frame. Fig. 17 shows the number of plastic hinges. A constant gravity load of $W_1 = 32$ kN/m was applied to the first to eighth stories and a constant gravity load of $W_2 = 28.7$ kN/m was applied to the beams of the roof. The seismic weight for the first story and roof was 1111 kN and 1176 kN, respectively, and for the second to eighth stories was 1092 kN. In order to find the optimal solution for the 9-story structure, a population of 80 and a maximum of 300 iterations were considered for the EWOA, ECBO and EVPS algorithms. The optimum sections and the best, worst, average, standard deviation and coefficient of variation of weights for the 9-story frame obtained from each of algorithms are presented in Table 4. The ratio of the best solution to those obtained from different optimization algorithms is shown in Fig. 18 for 30 independent runs. The difference between the best solution and those achieved by ECBO was less than for the two other algorithms, which shows the ability of this algorithm to find the optimal solution. This figure and Table 4 demonstrates that EWOA had more uniform performance in this example.

The lowest weight for the 9-story structure was 1326.49 kN and the optimum objective function value obtained by ECBO algorithm was 0.247.

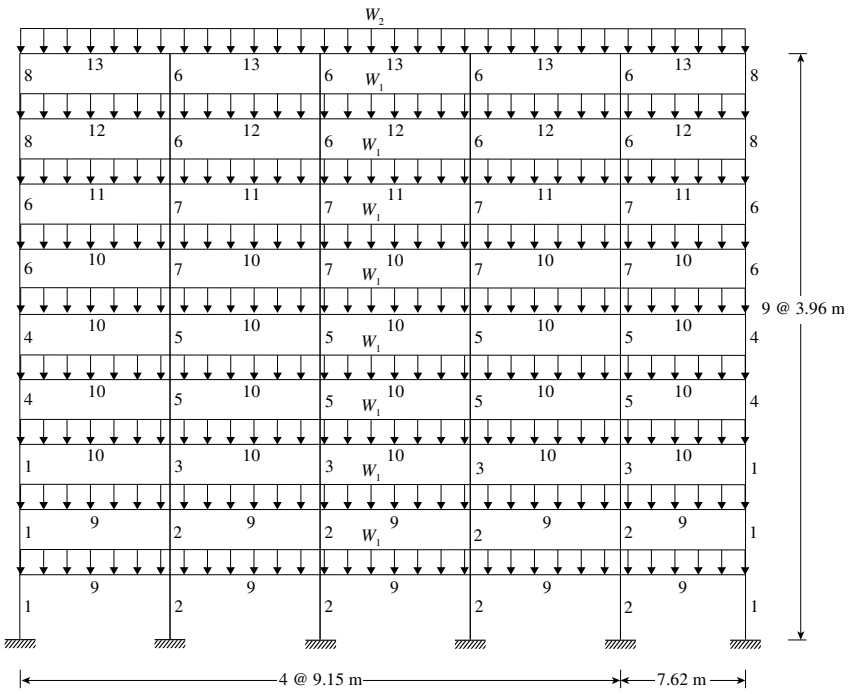

Fig. 16 Geometry, loading and grouping of elements of 9-story steel frame

Fig. 19 shows the plastic hinge formation patterns for the optimal solution of the 9-story frame using NSA with lateral loading pattern based on the first mode shape in positive and negative direction at each performance level. The ratio of plastic hinge rotations to their allowable values in FEMA 356 for a 9-story frame using the NSA with these load patterns is shown in Fig. 20. This ratio was less than unity for all plastic hinges, which indicates an acceptable amount of rotation (rotations of plastic hinges which were negligible are not shown).

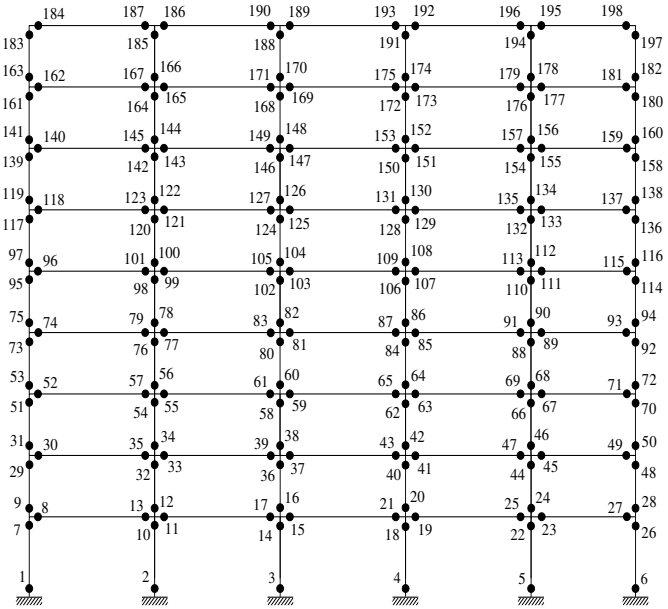

Fig. 17 Number of potential plastic hinges in 9-story steel frame

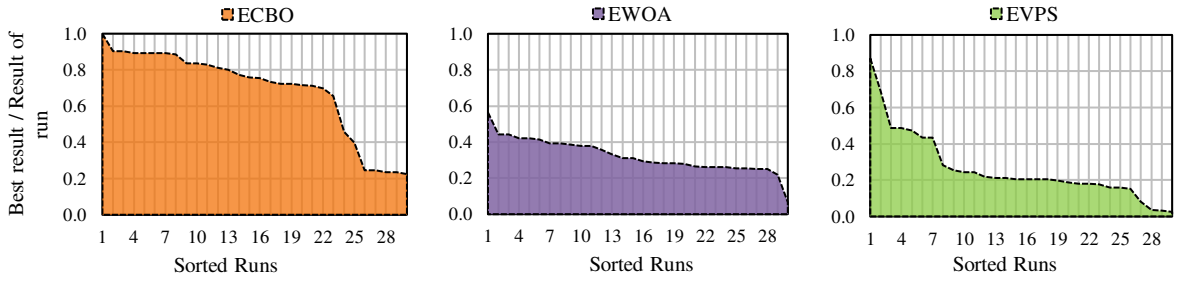

Fig. 18 Ratio of best solution to solutions of each algorithm for a 9-story steel frame

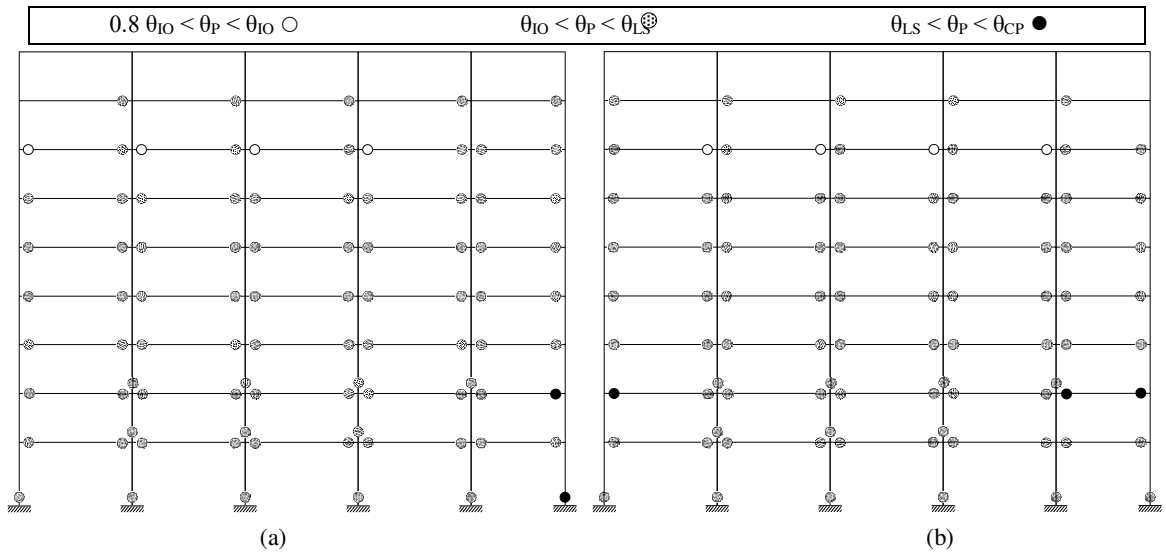

Fig. 19 Plastic hinges formation for a 9-story frame with lateral loading pattern based on the first mode shape in: (a) positive direction; (b) negative direction

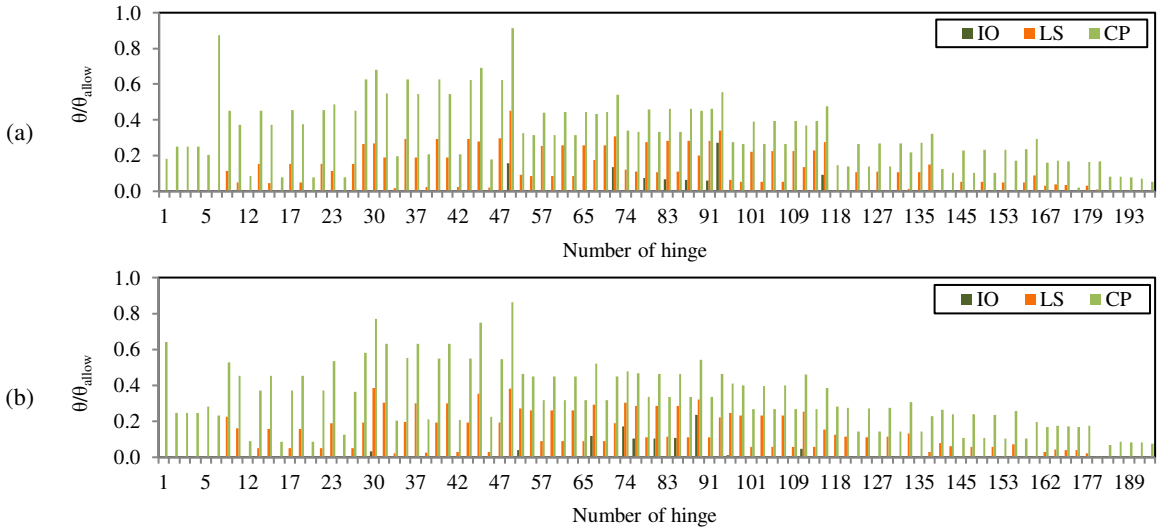

Fig. 20 Ratio of plastic rotation of hinges to their allowable values for a 9-story steel frame with lateral loading pattern based on the first mode shape in: (a) positive direction; (b) negative direction

Table 4 Optimal sections and weights for 9-story frame

Element group	ECBO	EVPS	EWOA
1	W 14 × 233	W 14 × 605	W 14 × 730
2	W 12 × 305	W 14 × 455	W 14 × 730
3	W 14 × 211	W 14 × 398	W 14 × 730
4	W 14 × 211	W 14 × 342	W 14 × 311
5	W 14 × 211	W 12 × 230	W 14 × 455
6	W 12 × 210	W 14 × 132	W 14 × 257
7	W 12 × 230	W 14 × 145	W 14 × 257
8	W 14 × 190	W 14 × 90	W 14 × 132
9	W 30 × 108	W 33 × 118	W 27 × 84
10	W 12 × 136	W 36 × 135	W 21 × 166
11	W 18 × 97	W 18 × 119	W 12 × 210
12	W 18 × 60	W 14 × 74	W 16 × 57
13	W 16 × 45	W 40 × 149	W 12 × 45
Best weight (kN)	1326.49	1655.38	2208.95
Worst weight (kN)	1994.12	1902.92	4170.48
Average weight (kN)	1480.96	1736.10	3559.40
Standard deviation of weights (kN)	270.45	180.05	352.45
Coefficient of variations (%)	18.28	11.72	9.90

The results of the formation pattern and plastic hinge rotation in the unsymmetrical 9-story structure at each performance level indicate that the use of NSA in only one direction is not sufficient and confirms the need for NSA in both directions. Fig. 21 compares the optimization convergence process of algorithms using the results obtained from optimization convergence of the best answer for each algorithm. Fig. 22 shows the displacement of stories, displacement-to-height ratio, and inter-story drift ratio of the structure for both load patterns. Comparison of the inter-story drift ratios and their permitted values for the best solution is shown in Fig 23.

5 Conclusions

A two-step approach has been proposed for PBD of unsymmetrical 2D SMRFs. In this approach, the structure is analyzed with lateral loading pattern based on the first mode shape in positive and negative direction. This means that the NSA should be performed in both directions. The objective function is formulated such that the difference between the successful and unsuccessful steps is taken into account and problem constraints are controlled for each performance level. The constraints in the second step depend on satisfying the constraints in the first step. The optimum designs for two case studies with unsymmetrical SMRFs having three and nine stories were performed using the meta-heuristic algorithms of EWOA, ECBO, EVPS, and SSA to evaluate the proposed approach.

The results showed that the EVPS showed greater ability for the three-story structure and ECBO performed uniformly when finding optimum solution for the nine-story structure, which led to the most desirable results. The pattern of plastic hinge formation and their rotation values for the unsymmetrical frames at each performance level confirmed that NSA should be performed in both directions. It is obvious that the proposed two-step approach for solving such problems can greatly reduce the computational volume by removing unnecessary calculations of nonlinear static analysis in the second step.

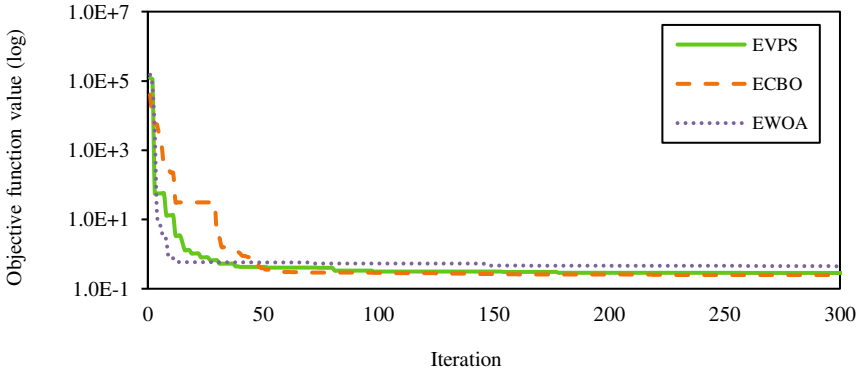

Fig. 21 Convergence curve of best solution of each algorithm for a 9-story steel frame

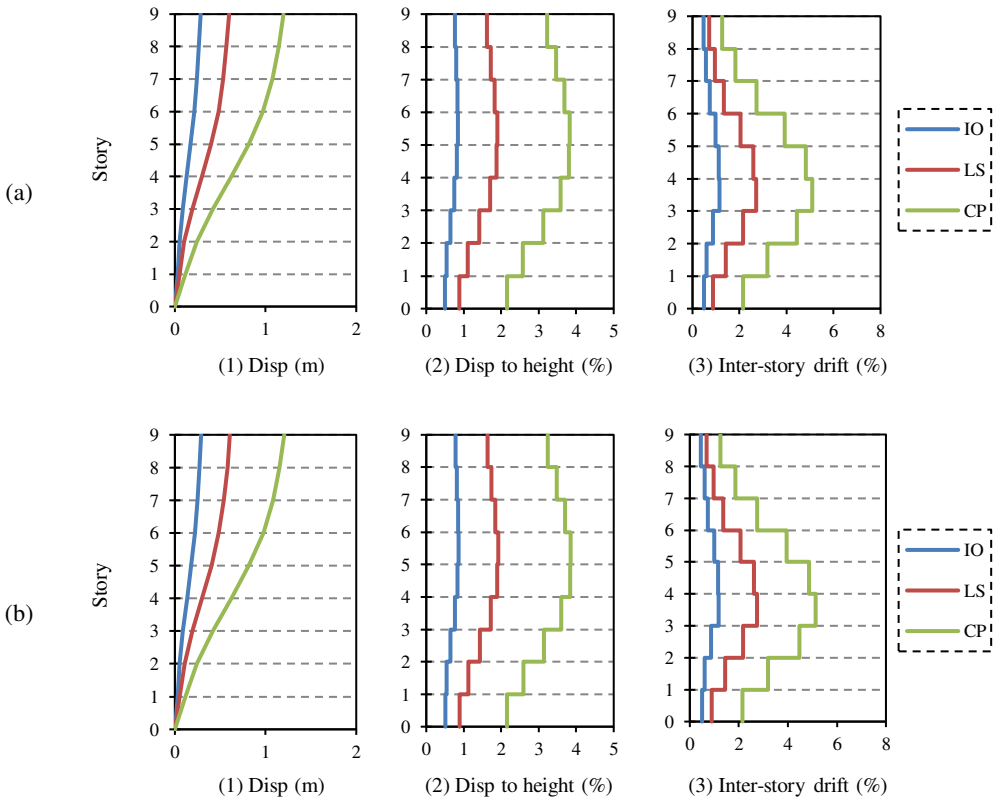

Fig. 22 Results of story drift for a 9-story steel frame with lateral loading pattern based on the first mode shape in: (a) positive direction; (b) negative direction

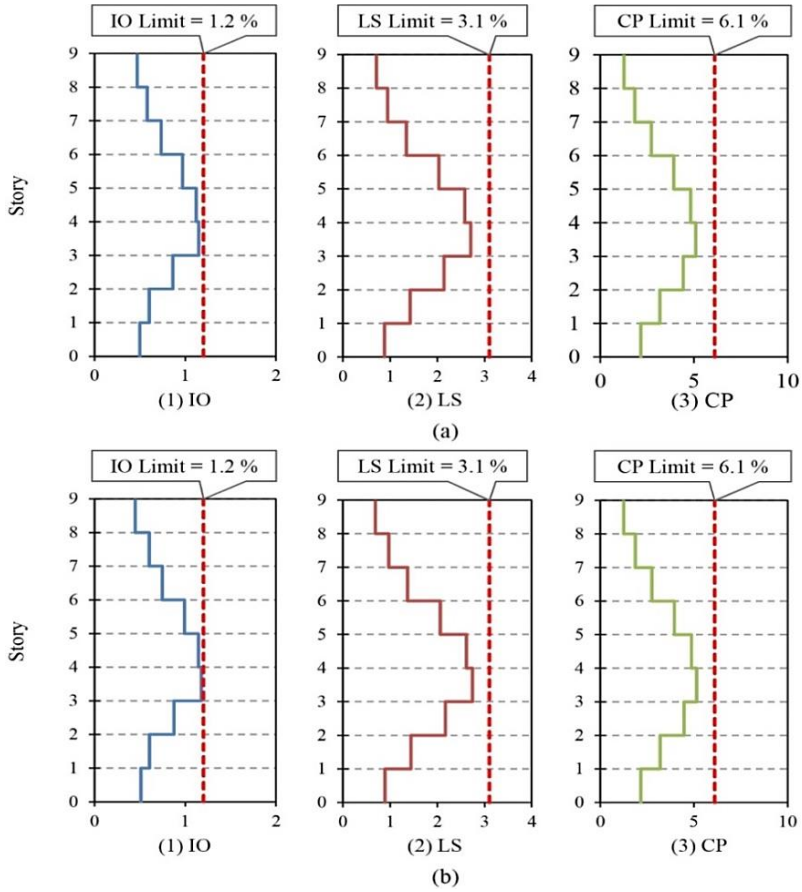

Fig. 23 Comparison of inter-story drift ratios (%) and their permitted values for the best solution for a 9-story steel frame with lateral loading pattern based on the first mode shape in: (a) positive direction; (b) negative direction

Declarations

Funding: Not applicable

Conflicts of interest/Competing interests: The authors declare that they have no conflict of interest.

Availability of data and material: Not applicable

Code availability: Not applicable

Authors' contributions: Study conception and design, Acquisition of data, Analysis and interpretation of data, Drafting of manuscript, Critical revision: A. Asaad Samani, S.R. Hoseini Vaez and M.A. Fathali

References

Aljarah I, Faris H, Mirjalili S (2018) Optimizing connection weights in neural networks using the whale optimization algorithm Soft Computing 22:1-15. https://doi.org/10.1007/s00500-016-2442-1

Anderson P, Bone Q (1980) Communication between individuals in salp chains. II. Physiology Proceedings of the Royal Society of London Series B Biological Sciences 210:559-574. https://doi.org/10.1098/rspb.1980.0153

Arora S, Singh S (2019) Butterfly optimization algorithm: a novel approach for global optimization Soft Computing 23:715-734. https://doi.org/10.1007/s00500-018-3102-4

Fathali MA, Hoseini Vaez SR (2020) Optimum performance-based design of eccentrically braced frames Engineering Structures 202:109857 https://doi.org/10.1016/j.engstruct.2019.109857

Fathollahi-Fard AM, Hajiaghaei-Keshteli M, Tavakkoli-Moghaddam R (2020) Red deer algorithm (RDA): a new nature-inspired meta-heuristic Soft Computing 24:14637-14665. https://doi.org/10.1007/s00500-020-04812-z

FEMA-356 (2000) Prestandard and commentary for the seismic rehabilitation of buildings. Federal

Emergency Management Agency, Washington, DC

Ghasemi-Marzbali A (2020) A novel nature-inspired meta-heuristic algorithm for optimization: bear smell search algorithm Soft Computing 24:13003-13035. https://doi.org/10.1007/s00500-020-04721-1

Gholizadeh S (2015) Performance-based optimum seismic design of steel structures by a modified firefly algorithm and a new neural network Adv Eng Softw 81:50-65. https://doi.org/10.1016/j.advengsoft.2014.11.003

Gholizadeh S, Baghchevan A (2017) Multi-objective seismic design optimization of steel frames by a chaotic meta-heuristic algorithm Engineering with Computers 33:1045-1060. https://doi.org/10.1007/s00366-017-0515-0

Gholizadeh S, Ebadijalal M (2018) Performance based discrete topology optimization of steel braced frames by a new metaheuristic Adv Eng Softw 123:77-92 https://doi.org/10.1016/j.advengsoft.2018.06.002

Gholizadeh S, Milani A (2016) Optimal performance-based design of steel frames using advanced metaheuristics Journal of Civil Engineering 17:607-623

Gholizadeh S, Poorhoseini H (2016a) Performance-Based Optimum Seismic Design of Steel Dual Braced Frames by Bat Algorithm. In: Yang X-S, Bekdaş G, Nigdeli SM (eds) Metaheuristics and Optimization in Civil Engineering. Springer International Publishing, Cham, pp 95-114. https://doi.org/10.1007/978-3-319-26245-1_5

Gholizadeh S, Poorhoseini H (2016b) Seismic layout optimization of steel braced frames by an improved dolphin echolocation algorithm Structural and Multidisciplinary Optimization 54:1011-1029. https://doi.org/10.1007/s00158-016-1461-y

Gong Y (2004) Performance-based design of steel building frameworks under seismic loading. University of Waterloo Ontario,

Grierson DE, Gong Y, Xu L (2006) Optimal performance-based seismic design using modal pushover analysis Journal of earthquake engineering 10:73-96

Hasan R, Xu L, Grierson DE (2002) Push-over analysis for performance-based seismic design Computers & Structures 80:2483-2493. https://doi.org/10.1016/S0045-7949(02)00212-2

Hassan R, Cohanim B, De Weck O, Venter G A comparison of particle swarm optimization and the genetic algorithm. In: 46th AIAA/ASME/ASCE/AHS/ASC structures, structural dynamics and materials conference, 2005. p 1897

Heidari AA, Faris H, Aljarah I, Mirjalili S (2019) An efficient hybrid multilayer perceptron neural network with grasshopper optimization Soft Computing 23:7941-7958. https://doi.org/10.1007/s00500-018-3424-2

Karimi F, Hoseini Vaez SR (2019) Two-stage optimal seismic design of steel moment frames using the LRFD-PBD method Journal of Constructional Steel Research 155:77-89. https://doi.org/10.1016/j.jcsr.2018.12.023

Kaveh A, Azar BF, Hadidi A, Sorochi FR, Talatahari S (2010) Performance-based seismic design of steel frames using ant colony optimization Journal of Constructional Steel Research 66:566-574. https://doi.org/10.1016/j.jcsr.2009.11.006

Kaveh A, Ghazaan MI (2017) A new meta-heuristic algorithm: vibrating particles system Scientia Iranica Transaction A, Civil Engineering 24:551

Kaveh A, Hoseini Vaez SR, Hosseini P (2017) Modified dolphin monitoring operator for weight optimization of frame structures Periodica Polytechnica Civil Engineering 61:770-779. https://doi.org/10.3311/PPci.9691

Kaveh A, Hoseini Vaez SR, Hosseini P (2018) Matlab code for an enhanced vibrating particles system algorithm International Journal of Optimization in Civil Engineering 8:401-414. http://ijoce.iust.ac.ir/article-1-352-fa.html

Kaveh A, Ilchi Ghazaan M (2014) Enhanced colliding bodies optimization for design problems with continuous and discrete variables Adv Eng Softw 77:66-75. https://doi.org/10.1016/j.advengsoft.2014.08.003

Kaveh A, Ilchi Ghazaan M (2017) Enhanced whale optimization algorithm for sizing optimization of skeletal structures Mechanics Based Design of Structures and Machines 45:345-362. https://doi.org/10.1080/15397734.2016.1213639

Kaveh A, Laknejadi K, Alinejad B (2012) Performance-based multi-objective optimization of large steel structures Acta Mech 223:355-369. https://doi.org/10.1007/s00707-011-0564-1

Kaveh A, Nasrollahi A (2014) Performance-based seismic design of steel frames utilizing charged system search optimization Applied Soft Computing 22:213-221. https://doi.org/10.1016/j.asoc.2014.05.012

LRFD-AISC (2001) Manual of steel construction- load and resistance factor design. In: LRFD-AISC. Third Edition edn. American Institute of Steel Construction (AISC), Chicago, Illinois, USA,

Madin LP (1990) Aspects of jet propulsion in salps Canadian Journal of Zoology 68:765-777. https://doi.org/10.1139/z90-111

Mazzoni S, McKenna F, Scott MH, Fenves GL (2005) OpenSees Command Language Manual.

University of California, . Pacific Earthquake Engineering Research (PEER) Center, Berkeley, California, USA

Mazzoni S, McKenna F, Scott MH, Fenves GL (2016) Open system for earthquake engineering simulation (OpenSees): version2.5.0. University of California, . Pacific Earthquake Engineering Research (PEER) Center, Berkeley, California, USA

Mergos PE (2018) Efficient optimum seismic design of reinforced concrete frames with nonlinear structural analysis procedures Structural and Multidisciplinary Optimization 58:2565-2581. https://doi.org/10.1007/s00158-018-2036-x

Mirjalili S, Gandomi AH, Mirjalili SZ, Saremi S, Faris H, Mirjalili SM (2017) Salp Swarm Algorithm: A bio-inspired optimizer for engineering design problems Adv Eng Softw 114:163-191. https://doi.org/10.1016/j.advengsoft.2017.07.002

Mirjalili S, Mirjalili SM, Lewis A (2014) Grey wolf optimizer Adv Eng Softw 69:46-61. https://doi.org/10.1016/j.advengsoft.2013.12.007

Mohammad Rezapour Tabari M, Hashempour M (2019) Development of GWO–DSO and PSO–DSO hybrid models to redesign the optimal dimensions of labyrinth spillway Soft Computing 23:6391-6406. https://doi.org/10.1007/s00500-018-3292-9

Shoeibi S, Kafi MA, Gholhaki M (2018) Performance-Based Seismic Design and Parametric Assessment of Linked Column Frame System Periodica Polytechnica Civil Engineering 62:555-569. https://doi.org/10.3311/PPci.10920

Figures

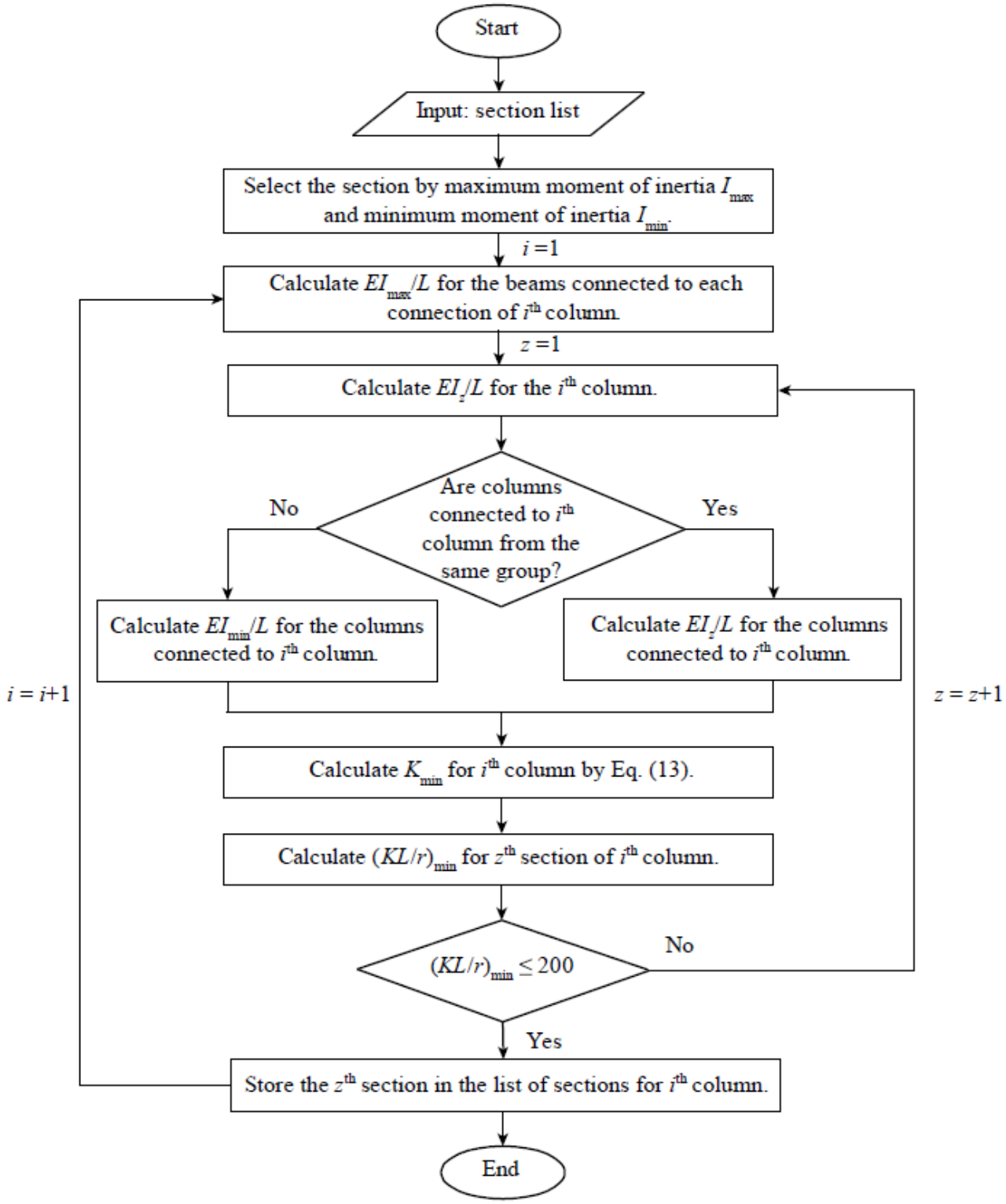

Figure 1

Flowchart for reducing the search space

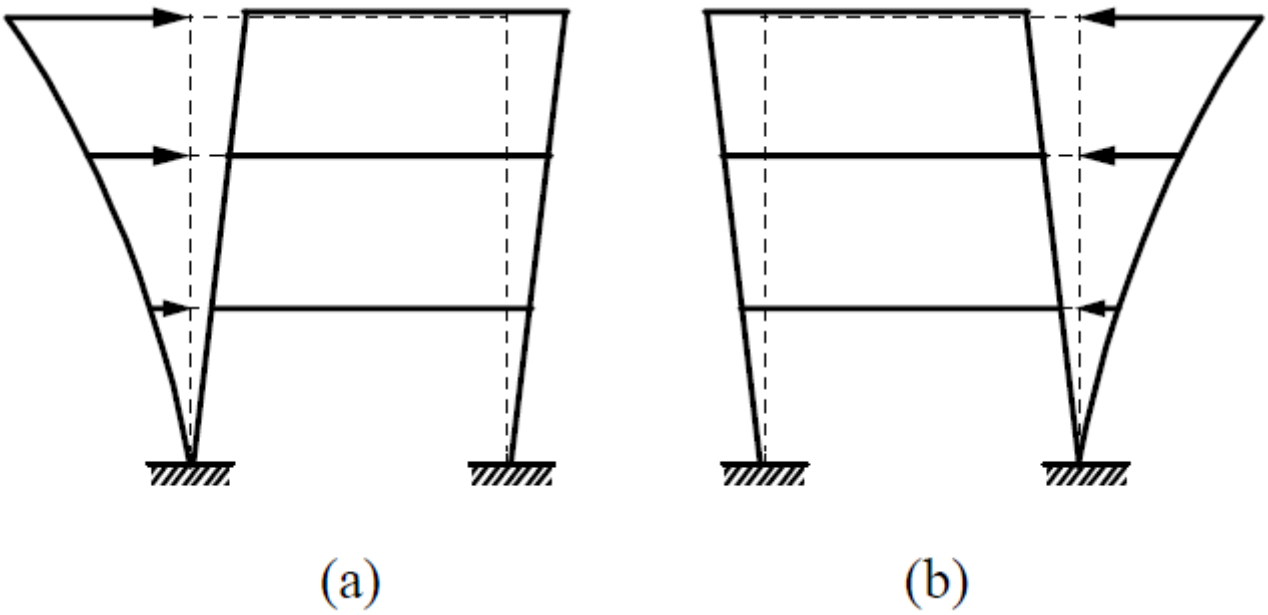

Figure 2

Lateral loading pattern based on the first mode shape (a) in positive direction and (b) in negative direction

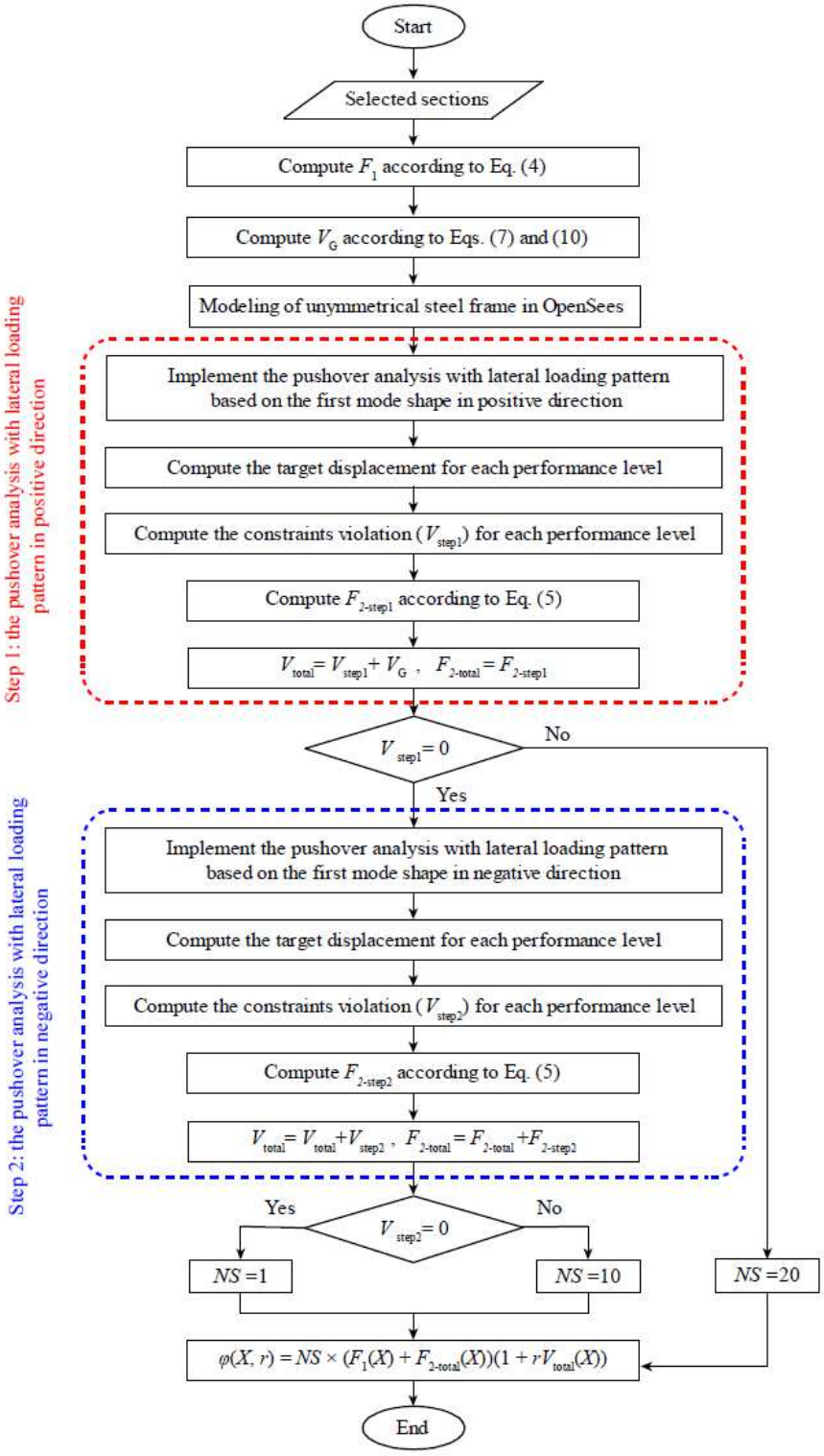

Figure 3

Flowchart of proposed approach

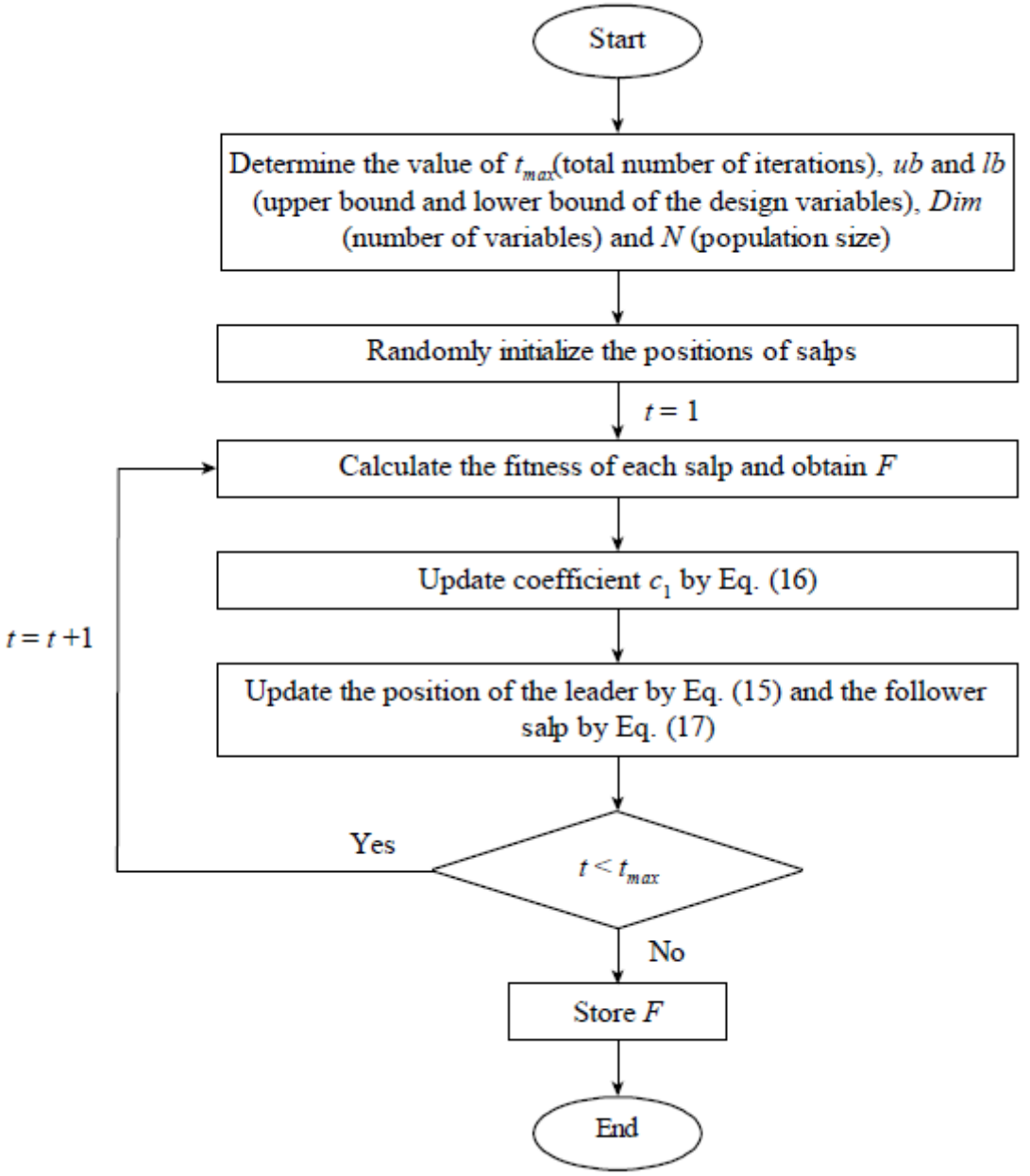

Figure 4

Flowchart of SSA algorithm

Determine the value of maximum number of iterations (t_{max}), population size (N) and colliding memory size.
Define the *Pro* in the [0, 1] range.
Initialize the position of CBs randomly in the search space.
While $t < t_{max}$
    Calculate the coefficient of restitution (ε) by Eq. (T1)*.
    Evaluate the objective function of CBs (f).
    Calculate the value of mass matrix (**m**) for the CBs using Eq. (T2).
    Update colliding memory and population.
    Divide CBs into stationary and moving groups and calculate their velocities before collision (**v**) by Eqs. (T3) and (T4).
    Calculate CBs velocities after the collision (**v'**) by Eqs. (T5) and (T6).
    Update the position of each CB by Eqs. (T7) and (T8).
    Select a random number (rni) that is distributed in the [0, 1] range.
    for i=**1**:N
        if rni<Pro
            Select one dimension of the i^{th} CB randomly and recalculate its value by Eq. (T9).
        end
    end
end
Report the best solution found by the algorithm.

* Eqs. (T1) to (T9) defined in Table 1

Figure 5

Pseudo-code for ECBO algorithm

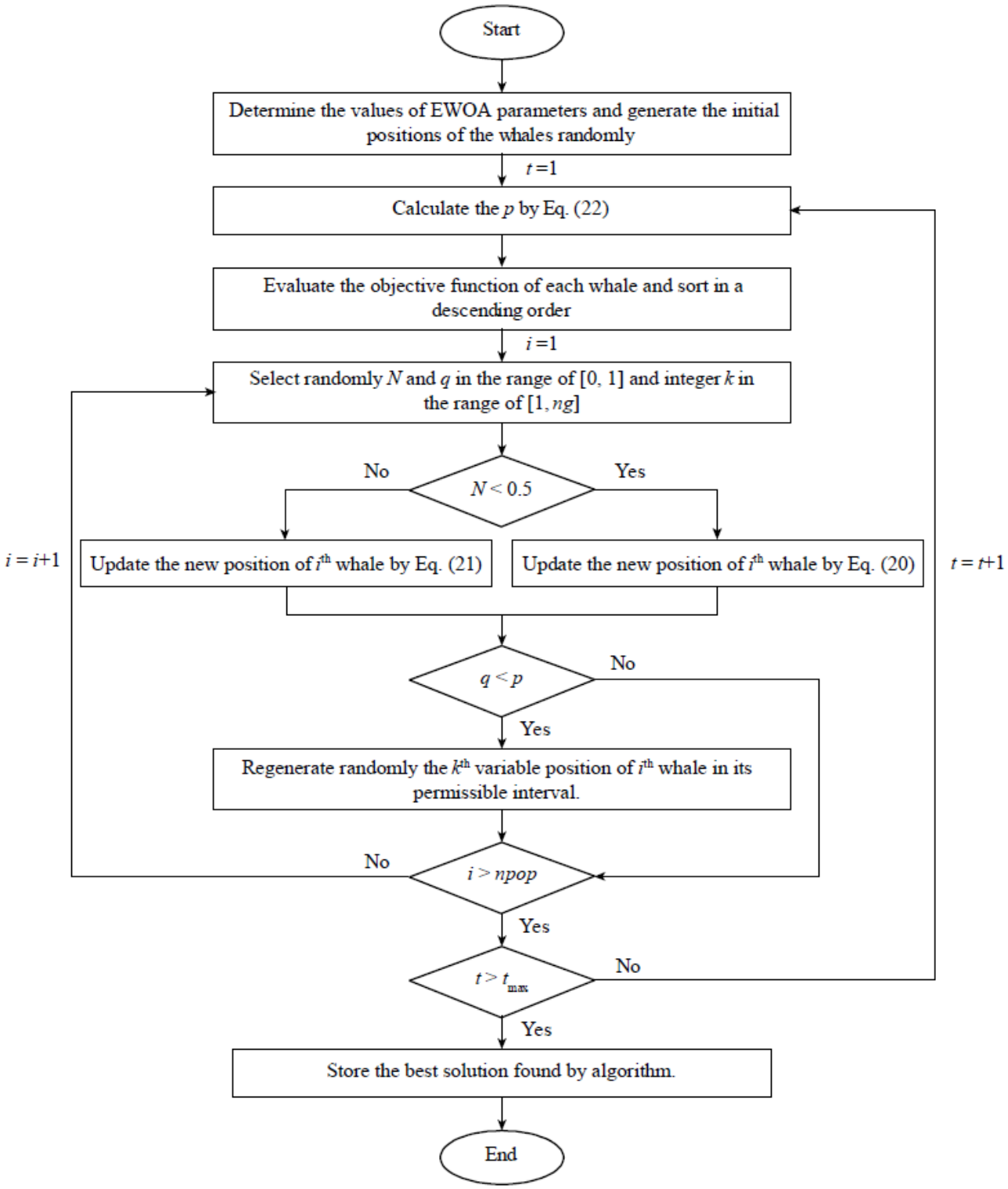

Figure 6

Flowchart of EWOA algorithm

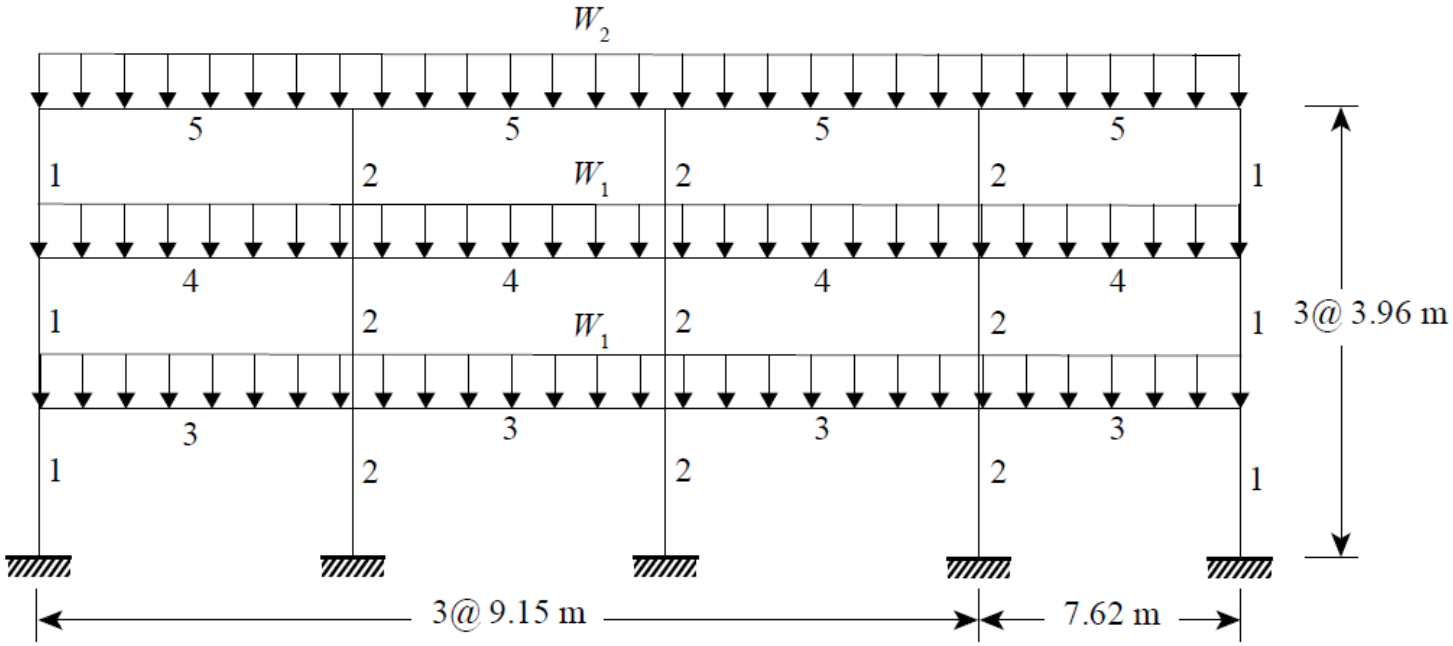

Figure 7

Geometry, loading and grouping of the elements of 3-story steel frame

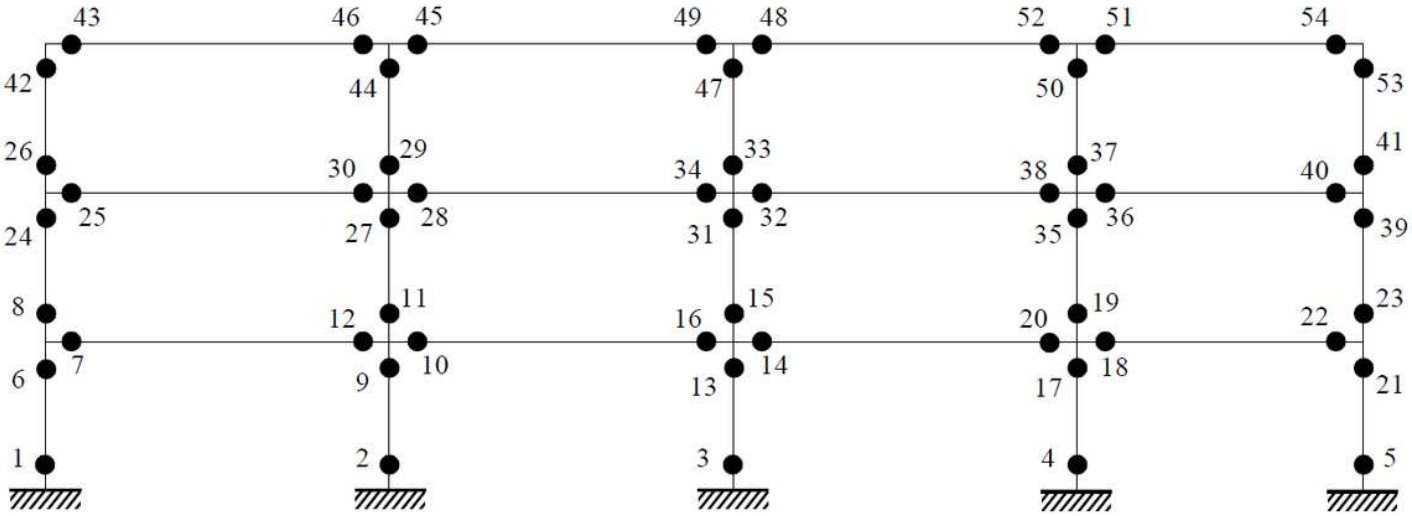

Figure 8

Number of potential plastic hinges in 3-story steel frame

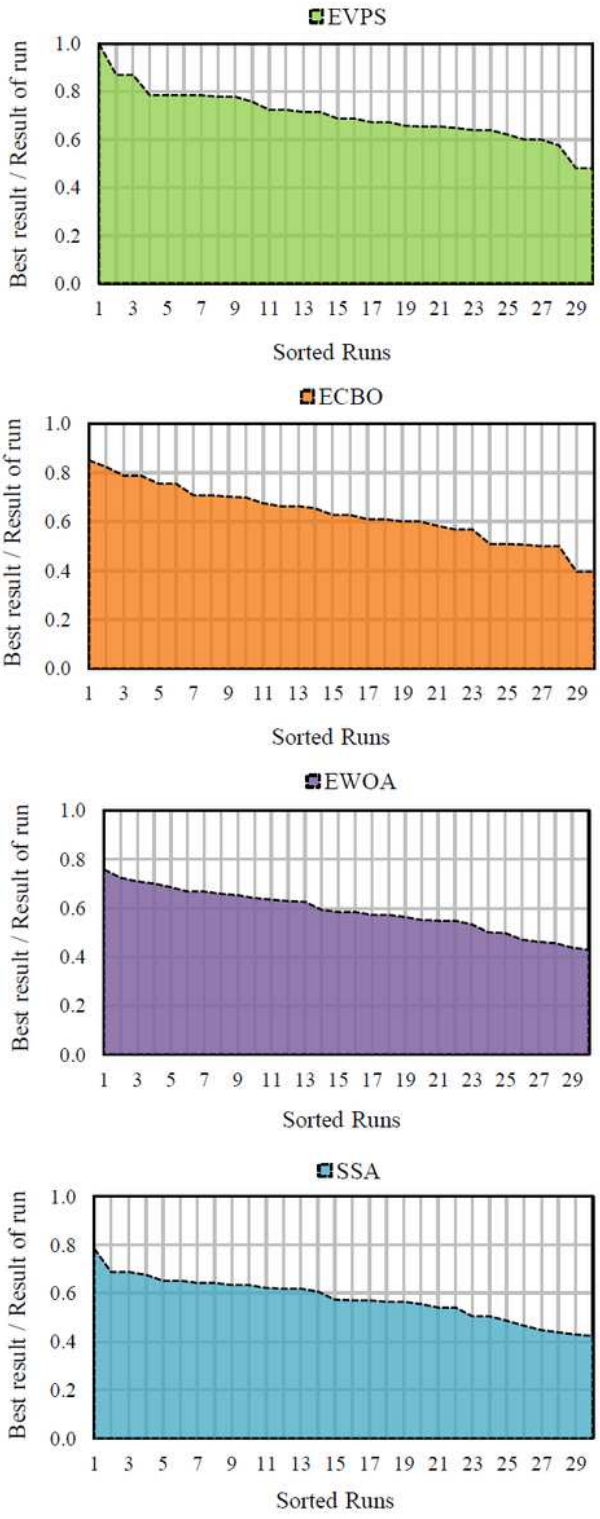

Figure 9

Ratio of best solution to solution of each algorithm for 3-story steel frame

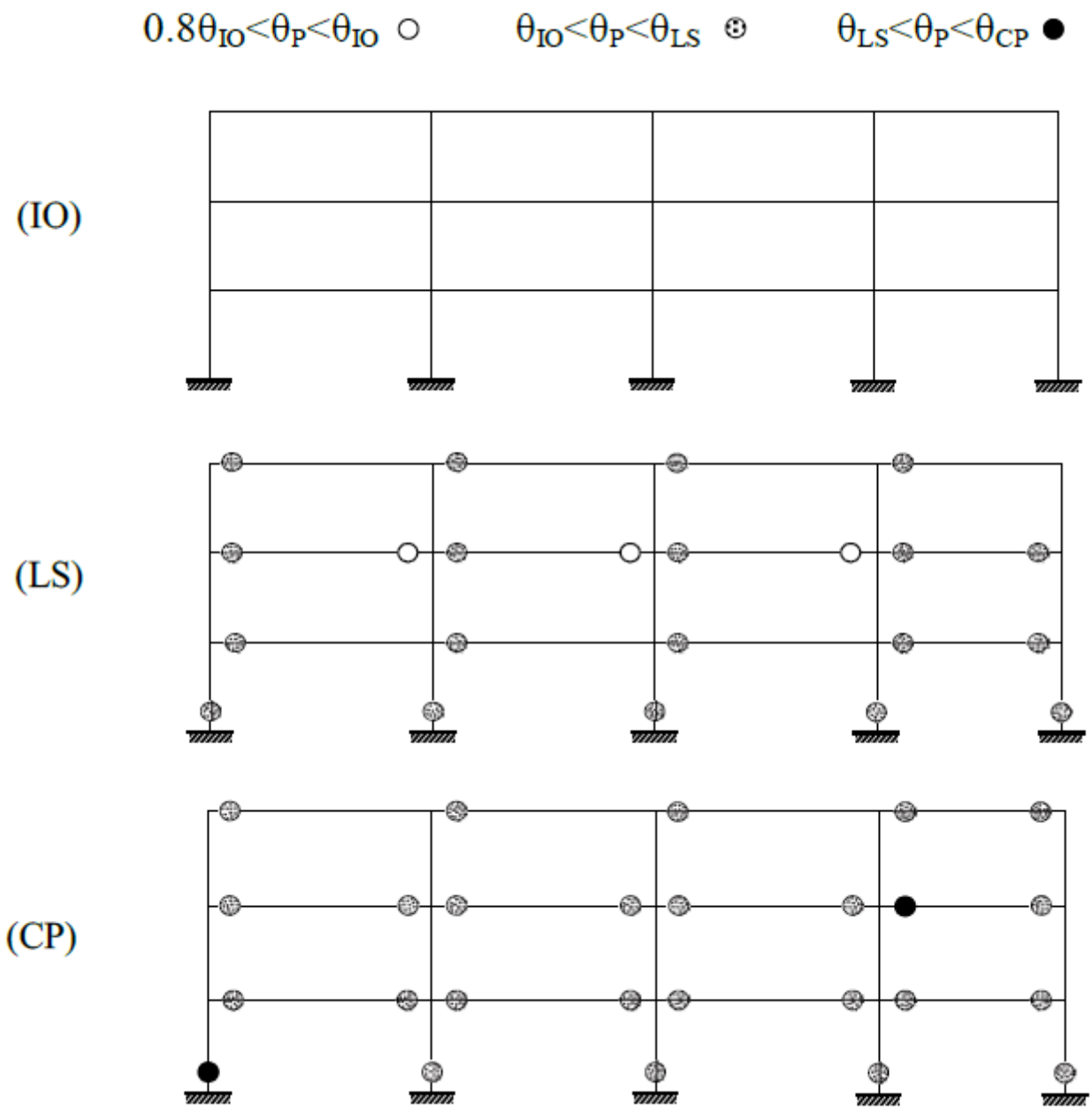

Figure 10

Plastic hinges formation for a 3-story frame with lateral loading pattern based on the first mode in positive direction

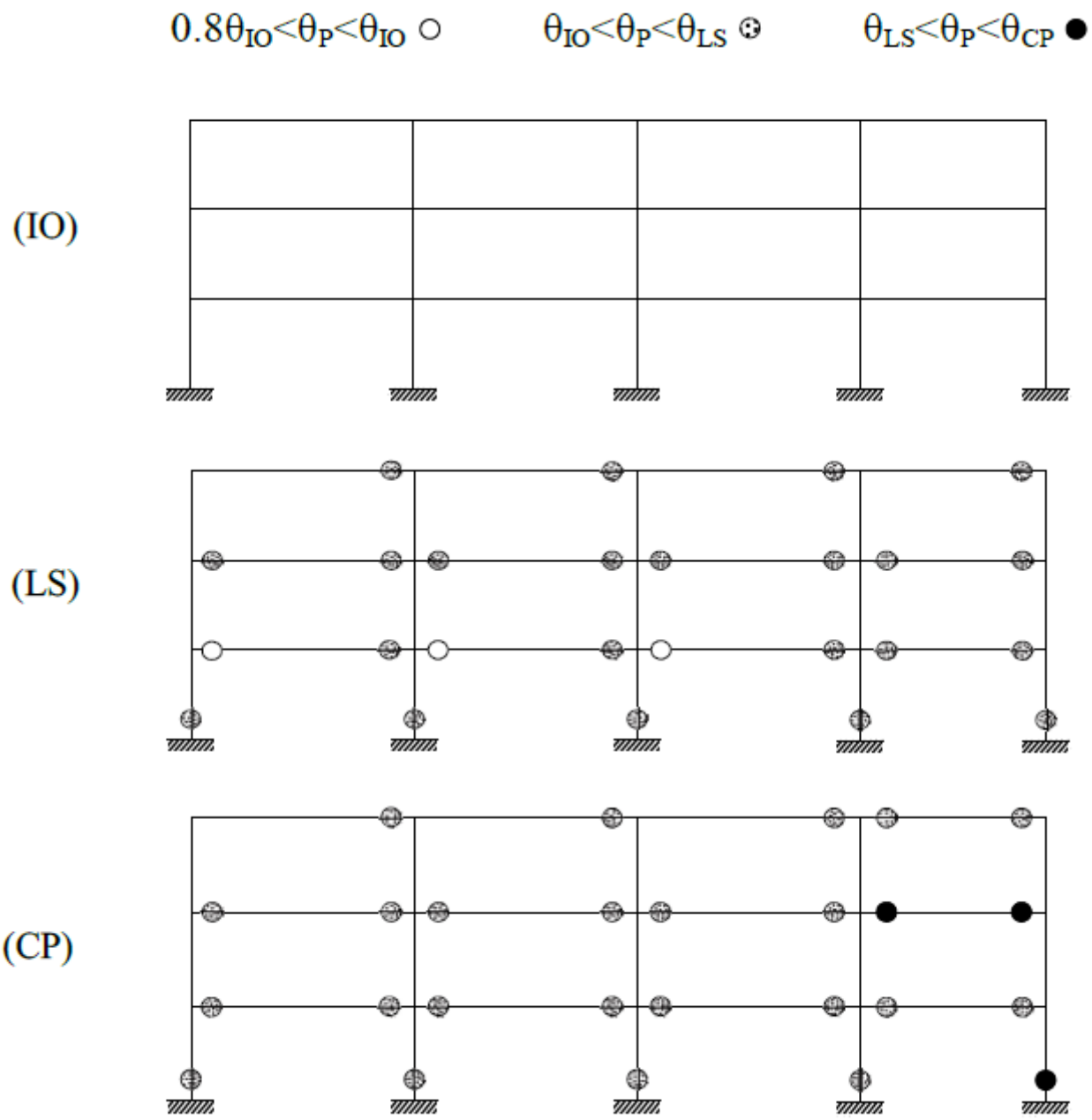

Figure 11

Plastic hinges formation for a 3-story frame with lateral loading pattern based on the first mode in negative direction

Figure 12

Ratio of plastic rotation of hinges to their allowable values for 3-story steel frame with lateral loading pattern based on the first mode shape in: (a) positive direction; (b) negative direction

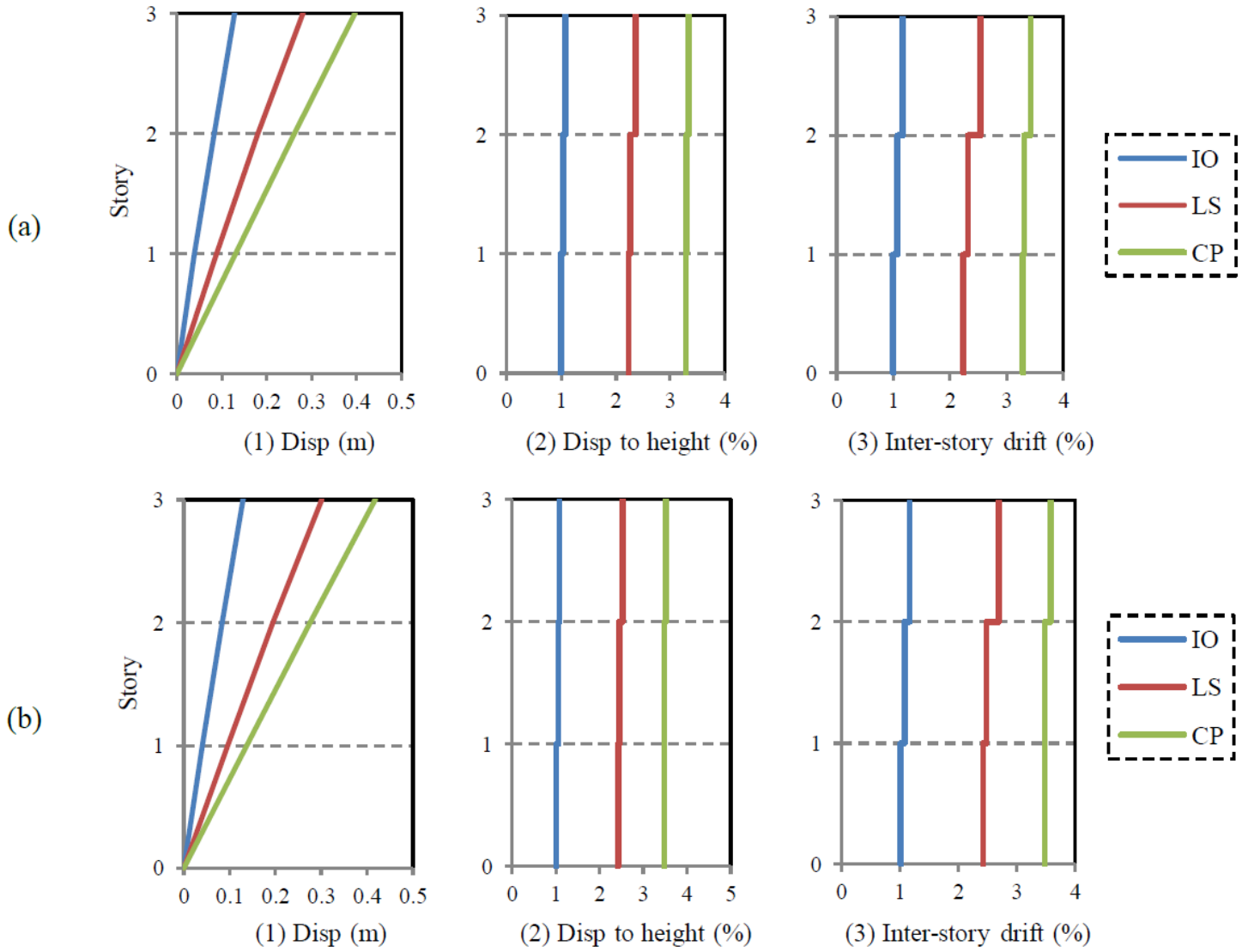

Figure 13

Results of story drift for 3-story frame with lateral loading pattern based on the first mode shape in: (a) positive direction; (b) negative direction

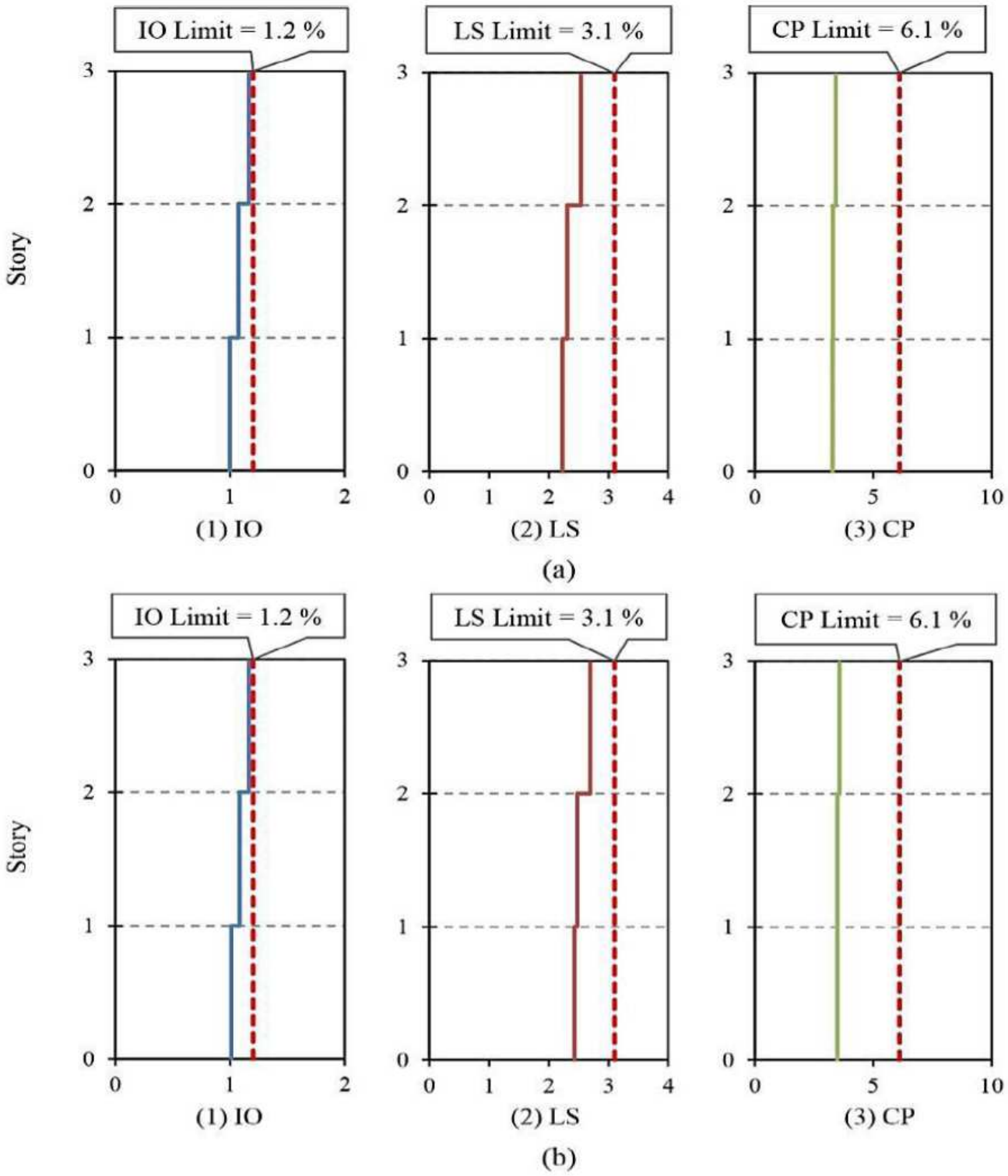

Figure 14

Comparison of inter-story drift ratios (%) and their permitted values for best solution for a 3-story steel frame with lateral loading pattern based on the first mode shape in: (a) positive direction; (b) negative direction

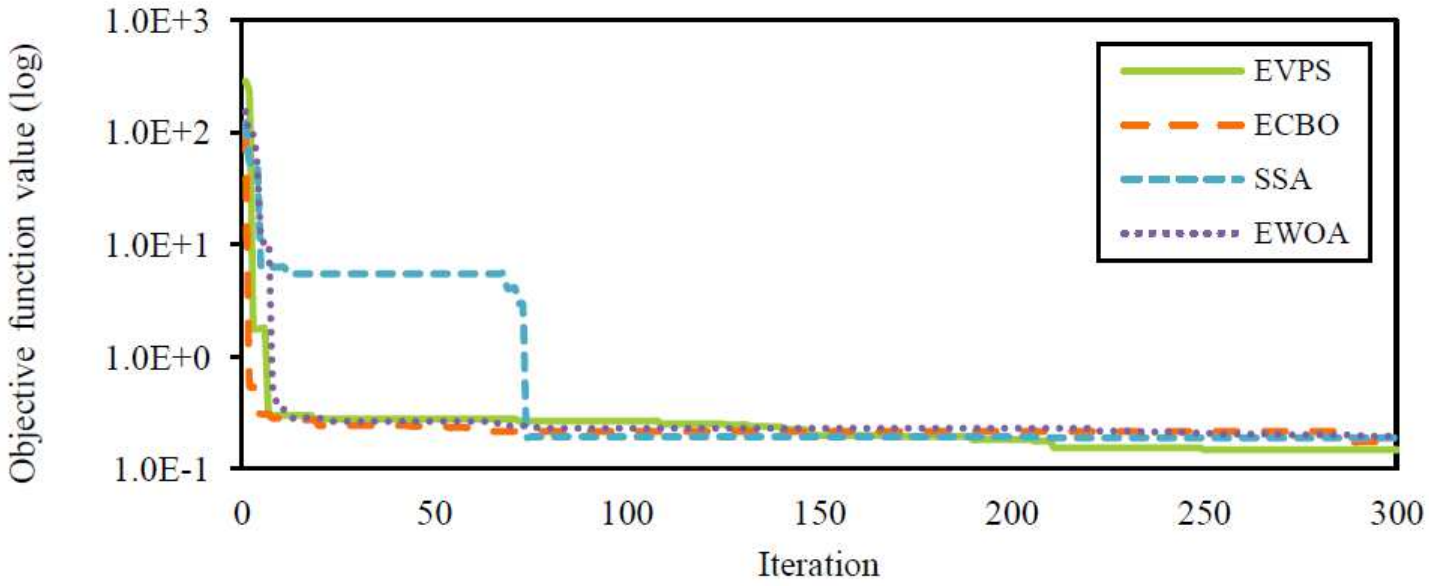

Figure 15

Convergence curve of best solution of each algorithm for 3-story steel frame

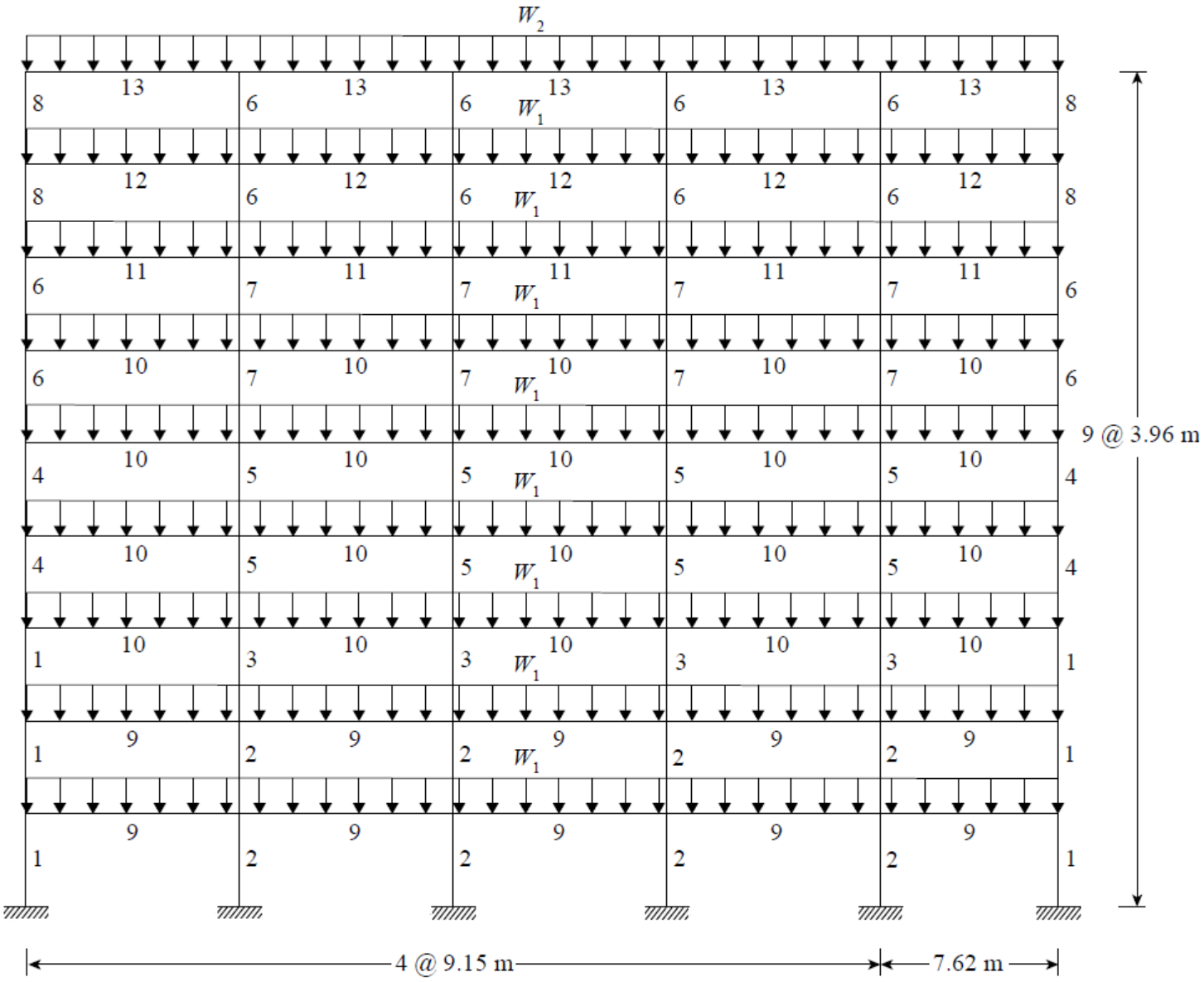

Figure 16

Geometry, loading and grouping of elements of 9-story steel frame

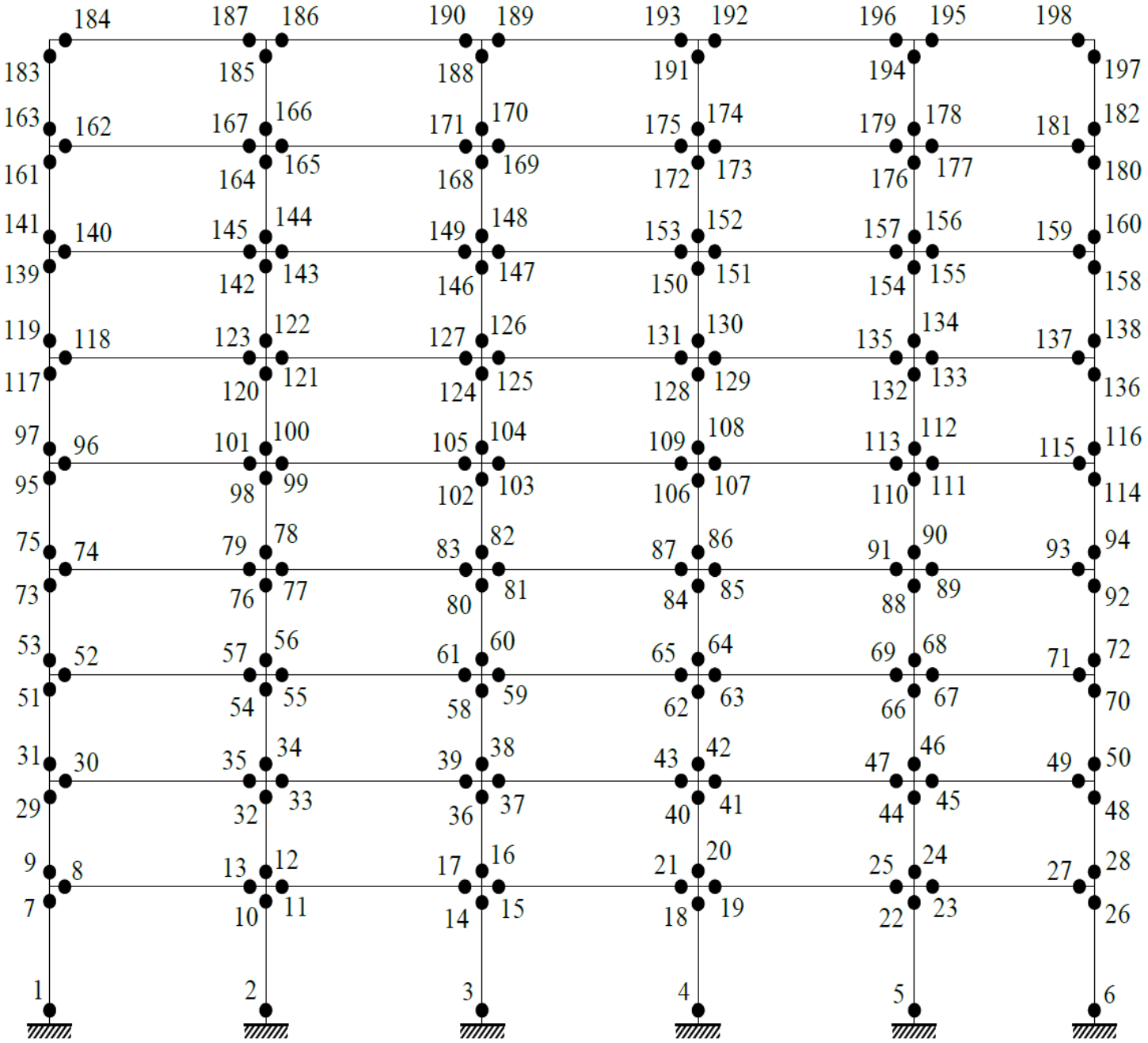

Figure 17

Number of potential plastic hinges in 9-story steel frame

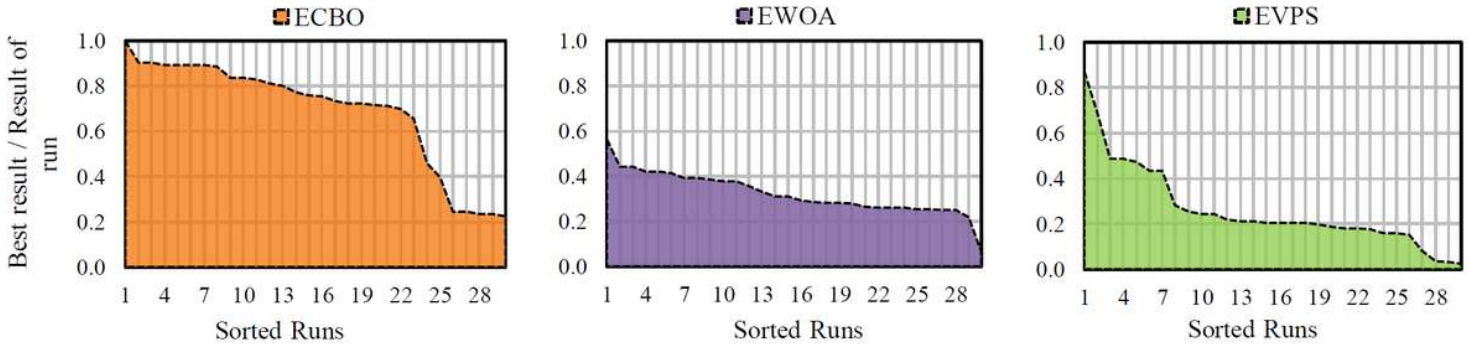

Figure 18

Ratio of best solution to solutions of each algorithm for a 9-story steel frame

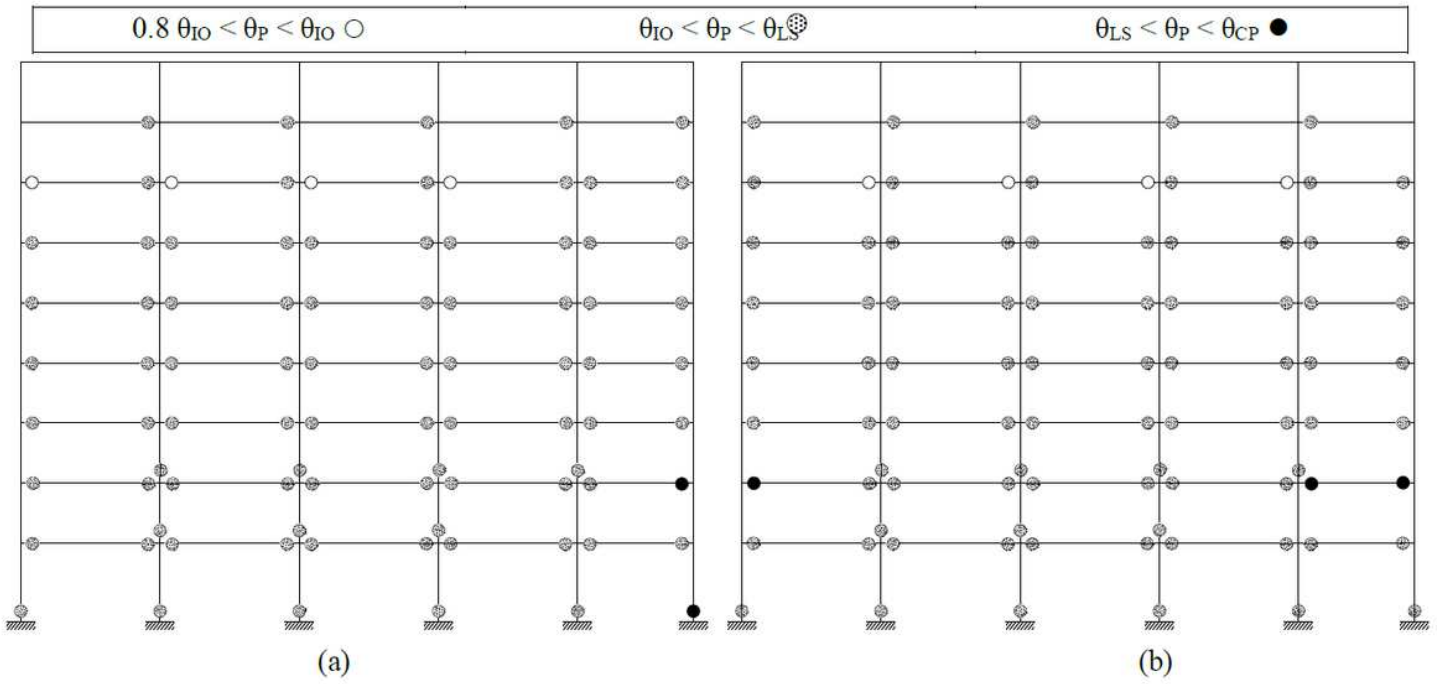

Figure 19

Plastic hinges formation for a 9-story frame with lateral loading pattern based on the first mode shape in: (a) positive direction; (b) negative direction

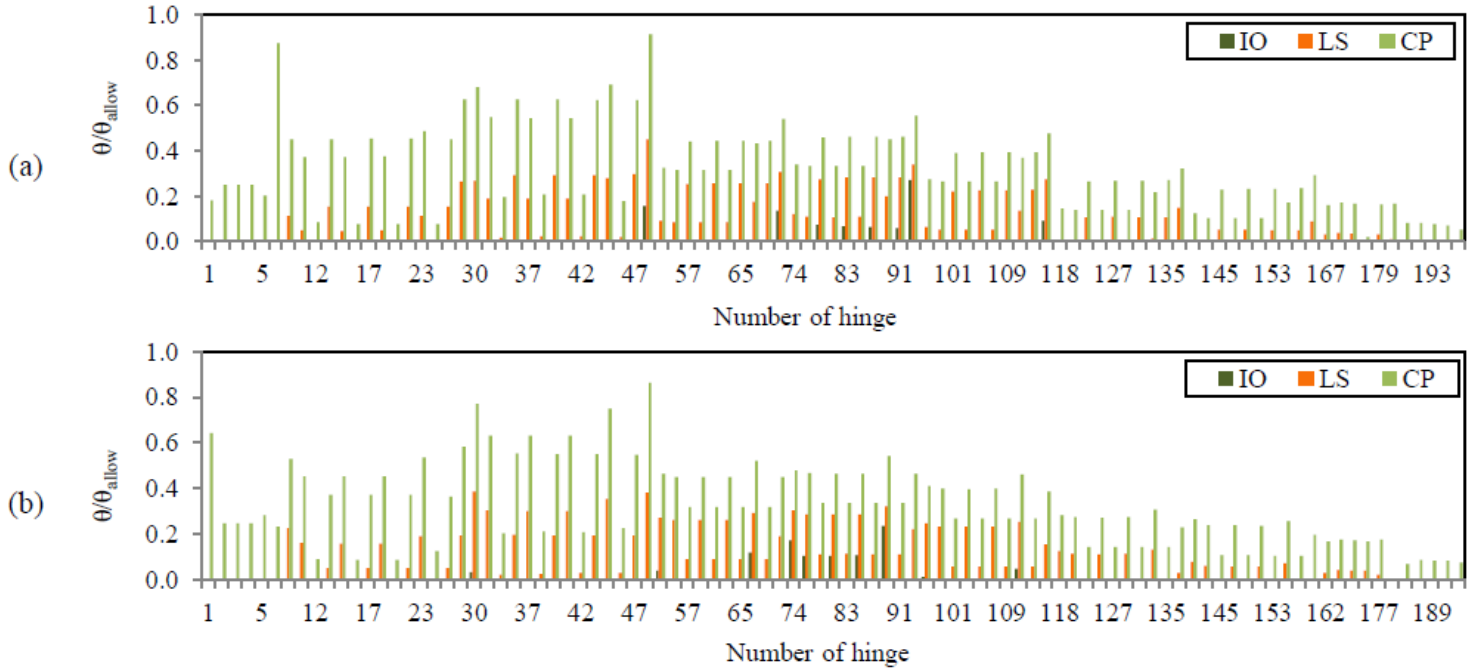

Figure 20

Ratio of plastic rotation of hinges to their allowable values for a 9-story steel frame with lateral loading pattern based on the first mode shape in: (a) positive direction; (b) negative direction

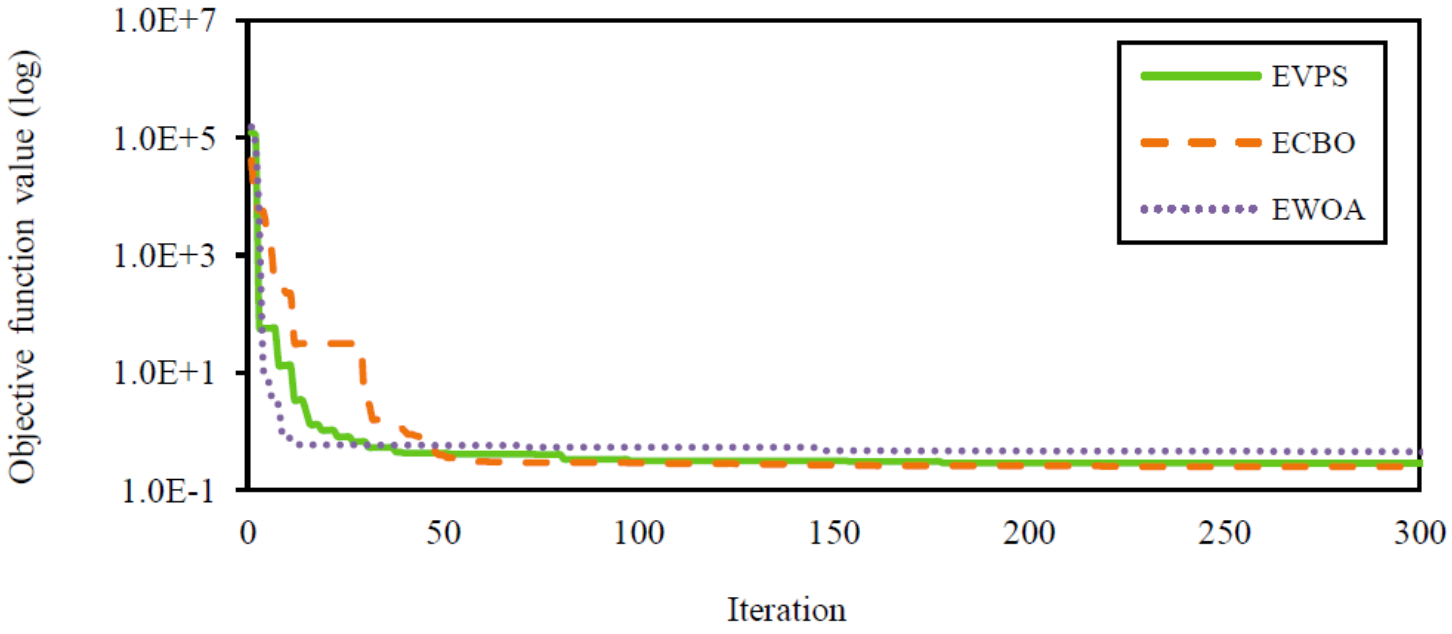

Figure 21

Convergence curve of best solution of each algorithm for a 9-story steel frame

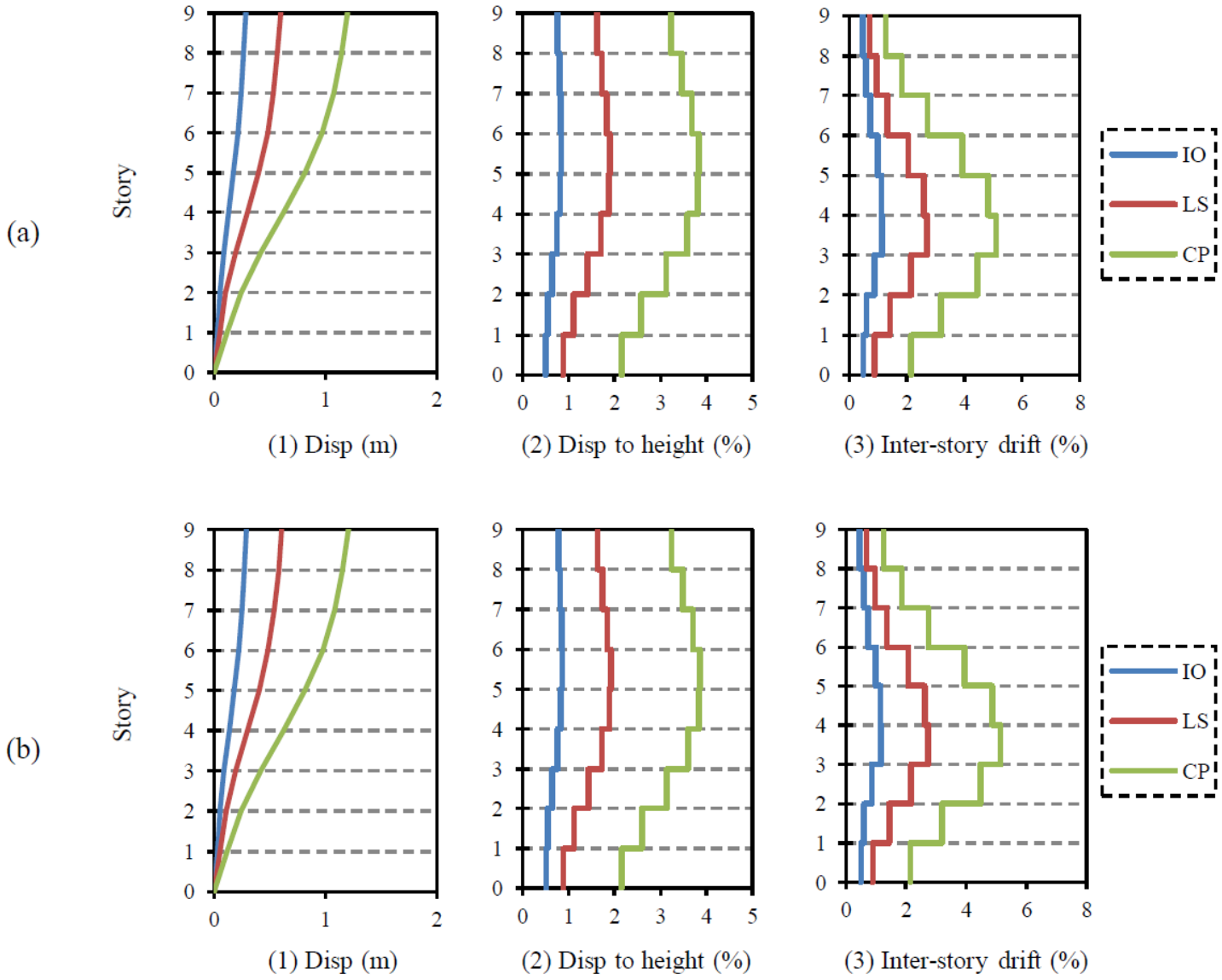

Figure 22

Results of story drift for a 9-story steel frame with lateral loading pattern based on the first mode shape in: (a) positive direction; (b) negative direction

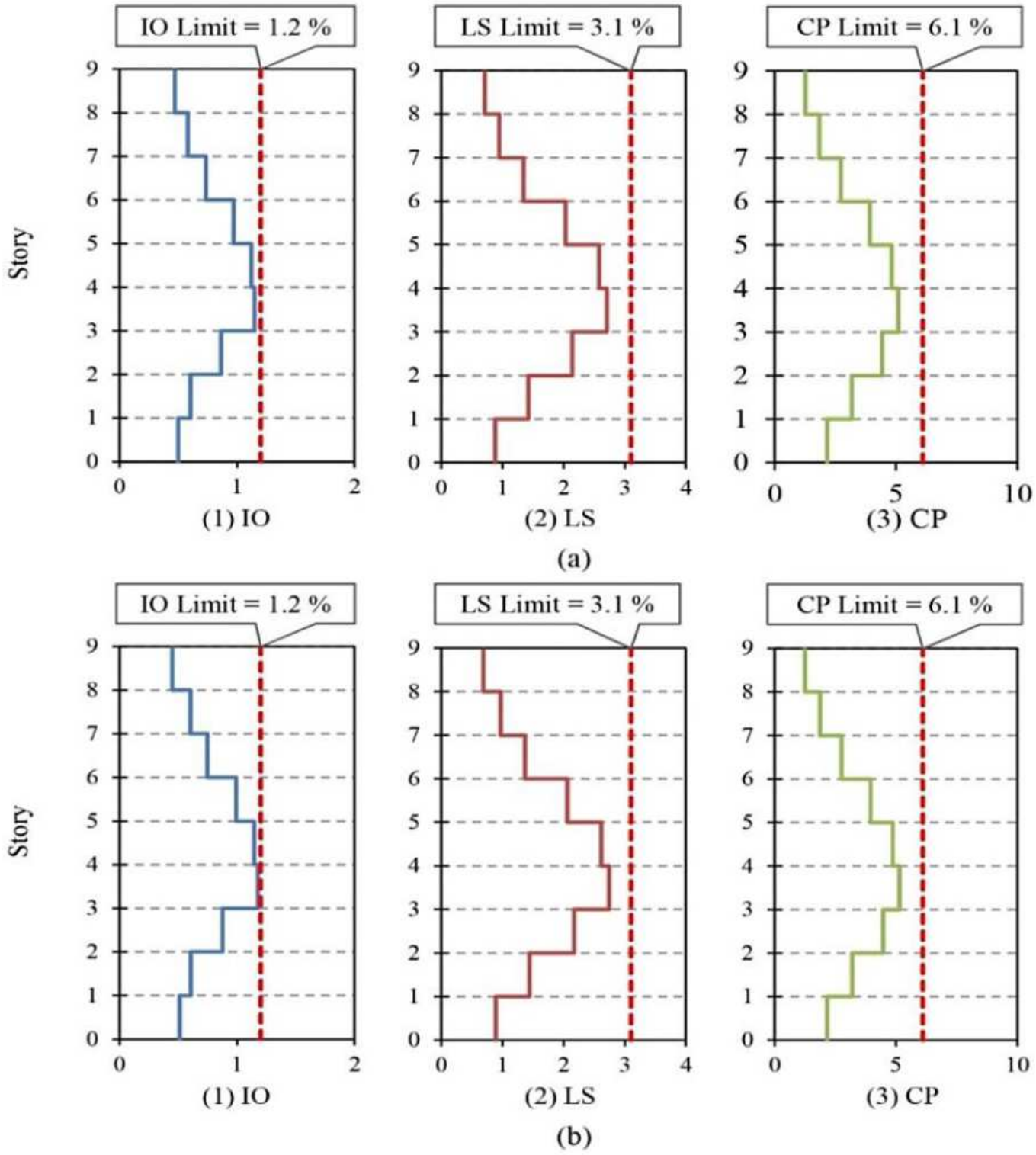

Figure 23

Comparison of inter-story drift ratios (%) and their permitted values for the best solution for a 9-story steel frame with lateral loading pattern based on the first mode shape in: (a) positive direction; (b) negative direction